Transactions of the Royal Society of Edinburgh: Earth Sciences, **95**, 491–510, 2005 (for 2004)

Archaean crust in the Rayner Complex of east Antarctica: Oygarden Group of islands, Kemp Land

N. M. Kelly, G. L. Clarke and C. M. Fanning

ABSTRACT: Archaean zircon grains from the Oygarden Group of islands in Kemp Land, east Antarctica, record evidence for multiple episodes of recrystallisation, dissolution and growth from the Early to Middle Archaean to the Neoproterozoic. Zircon grains in layered felsic orthogneiss have an age of ~3650 Ma, a minimum protolith age for this rock. These zircon grains were subsequently affected by a ~3470 Ma Pb-loss event. Homogeneous felsic orthogneiss that cuts S_1, but contains an intense S_2 foliation, has disturbed ~2780 Ma metamorphic zircon cores and rims that suggest a minimum age of ~2780 Ma for the protolith to the orthogneiss. All zircon U-Pb data display considerable disturbance with further Pb-loss at ~2400 Ma and ~1600 Ma, and a major episode of isotopic resetting at ~930 Ma. The highly disturbed data are related to complexly zoned zircon grains that developed through growth and modification during successive metamorphic events. Zircon cores with relic growth zoning patterns are inferred to have resulted from partial annealing or recrystallisation of older magmatic zircon. Highly luminescent zircon rims that embay cores along curved boundaries are interpreted to have formed through recrystallisation of zircon cores, and not new growth. The ages reported here confirm that central Kemp Land is composed of Archaean crust reworked during the Neoproterozoic Rayner Structural Episode.

KEY WORDS: granulite facies, Pb-loss, recrystallisation, U-Pb geochronology, zircon.

The widespread use of imaging techniques such as back scattered electron (BSE) and cathodoluminscence (CL) imaging has provided insights into the complex internal zoning within zircon grains that reflect stages of growth and/or recrystallisation (Vavra 1990; Hanchar & Miller 1993; Koschek 1993). For example, the character of internal zoning patterns has been used to infer a magmatic (Vavra 1990; Mezger & Krogstad 1997) or 'metamorphic' (Watson & Liang 1995; Vavra *et al.* 1996; Mezger & Krogstad 1997; Schaltegger *et al.* 1999; Rubatto & Gebauer 2000; Kelly & Harley 2005) growth origin of zircon. Moreover, CL/BSE techniques may aid us in discriminating different growth environments of 'metamorphic' zircon, including through sub-solidus reaction (Hanchar & Rudnick 1995; Watson & Liang 1995; Vavra *et al.* 1996; Fraser *et al.* 1997; Schaltegger *et al.*, 1999) or growth in the presence of partials melts (Vavra *et al.* 1996; Roberts & Finger 1997; Schaltegger *et al.* 1999; Rubato & Gebauer 2000; Kelly *et al.* 2002; Kelly & Harley 2005). As such, the integration of CL and BSE imaging with microbeam analysis has revealed considerable complexity in zircon grains formed during mono- and poly-cyclic metamorphism (Black *et al.* 1986; Williams 1992; Vavra *et al.* 1996, 1999; Kelly & Harley 2005).

Importantly, CL and BSE imaging has been able to identify post-crystallisation modification of zircon. For example, the damage to the zircon lattice caused during metamictisation is thought to produce a subdued CL response in comparison to non-metamict zones (Koschek 1993; McLaren *et al.* 1994). Such zones are not only more susceptible to Pb-loss (Cherniak *et al.* 1991; Mezger & Krogstad 1997; Meldrum *et al.* 1998; Geisler *et al.* 2002), but may induce matrix effects during ion probe analysis that create erroneous data (McLaren *et al.* 1994; Black *et al.* 1986). Equally as important in metamorphic terranes, is the ability to recognise zircon that has been modified during metamorphic or fluid events that may post-date magmatic or metamorphic zircon growth. Annealing of a previously damaged (metamict) or strained zircon lattice, which may be accompanied by isotopic disturbance through enhanced diffusion of U–Th–Pb, can cause blurring and partial erasure of primary zoning features (Schaltegger *et al.* 1999). In addition, the replacement of primary growth zoning may occur through a process of recrystallisation. Recrystallisation may involve the development of curved embayments that resemble a chemical reaction front (Harley *et al.* 1998; Schaltegger *et al.* 1999; Vavra *et al.* 1999; Hoskin & Black 2000), preferential replacement controlled and guided by primary structures (Vavra *et al.* 1999), or recrystallisation along and partial to complete healing of fracture networks within zircon grains (Hartmann *et al.* 1997). Recrystallisation may be driven by hydrothermal/metasomatic fluids (Pidgeon 1992; Pidgeon *et al.* 1998; Rubatto & Gebauer 2000; Carson *et al.* 2002b; Tomaschek *et al.* 2003), will typically cause enhanced mobility of trace elements and U–Th–Pb (Schaltegger *et al.* 1999; Vavra *et al.* 1999; Hoksin & Black 2000), and can result in enhanced or lower luminescence relative to primary features in the zircon grain. Recognition of such zones is therefore highly important not only to distinguish them from primary growth features, but also to allow more informed interpretation of age data from such multi-phase zircon grains.

In mono- and poly-cyclic metamorphic terranes, thermal and fluid events may lead to successive episodes of dissolution, new zircon growth or recrystallisation of zircon grains. The ability to identify these features using imaging and microbeam techniques has allowed tighter constraints to be placed on the magmatic and *P–T–t* evolution of many mountain belts (Rubatto *et al.* 1999; Schaltegger *et al.* 1999; Vavra *et al.* 1999; Zeck & Whitehouse 1999; Hermann *et al.* 2001). Moreover, these techniques have allowed discrimination between thermal and fluid events (Vavra *et al.* 1999; Tomaschek *et al.* 2003). However, in some terranes, modification of zircon or the

https://doi.org/10.1017/S0263593300001176 Published online by Cambridge University Press

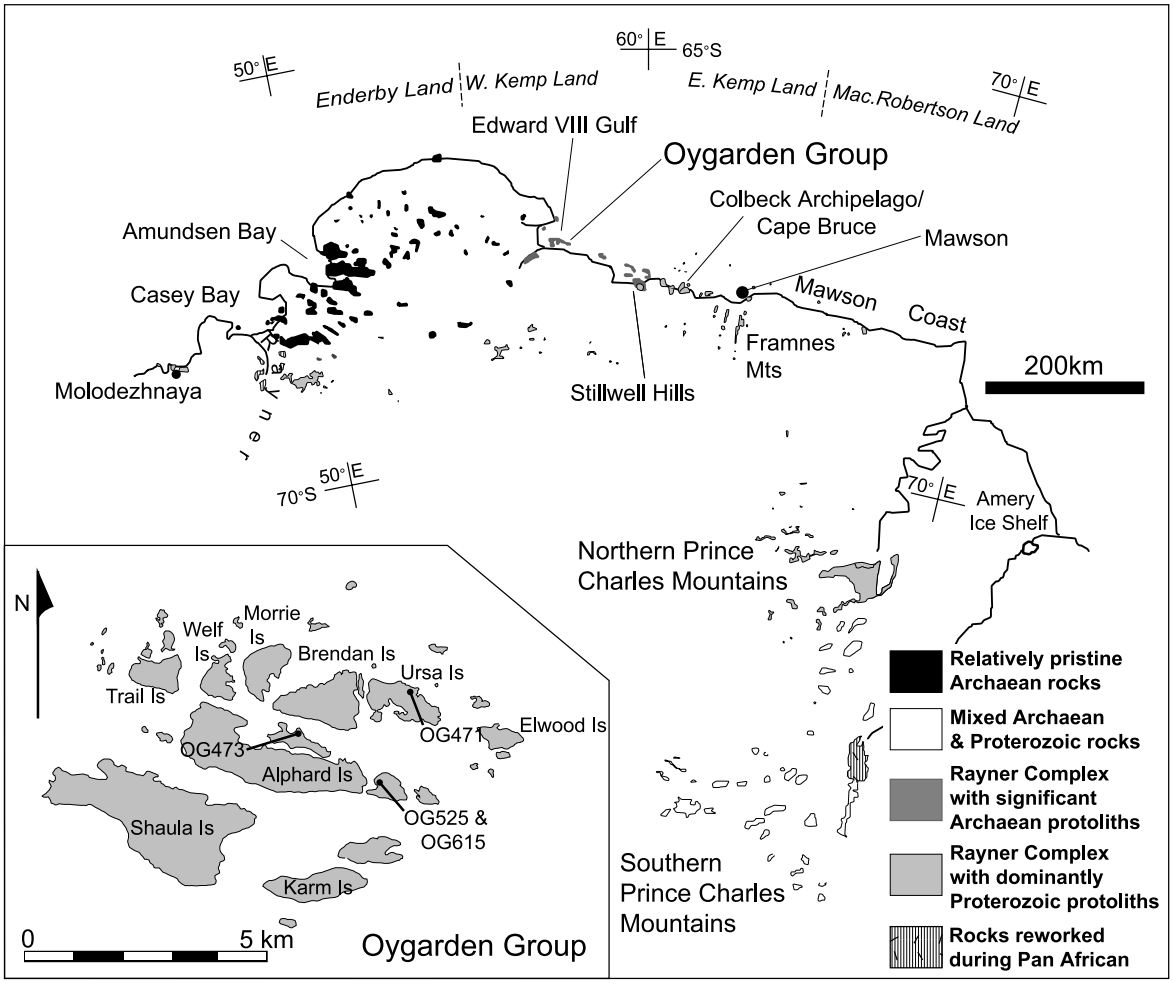

Figure 1 Location and outcrop map of Enderby, Kemp and MacRobertson Lands, showing the location of the Oygarden Group of Islands. *Inset*: central islands of the Oygarden Group, showing the location of the samples discussed in this paper (GPS locations of samples are provided in the text).

development of recrystallised rims on older zircon cores during metamorphism may result in varying intensity of resetting of isotopic systems, where the 'new' or modified zircon retains an isotopic 'memory' of the older zircon material, the degree to which will be dependent on the intensity of recrystallisation (Harley *et al.* 1998; Harley & Black 1997; Hoskin & Black 2000; Carson *et al.* 2002b). Where variable resetting occurs during a single event, upper and lower intercepts of discordia may be attributed geological events (Mezger & Krogstad 1997; Harley *et al.* 1998; Carson *et al.* 2002b). However, multiple stages of incomplete resetting and Pb-loss during successive events may generate complex data sets that render a 'grouped age' statistical approach geologically meaningless (Mezger & Krogstad 1997). The development of such complex data sets underlies the need for the careful interpretation of internal zircon textures and the requirement for an integrated analytical approach.

This paper builds on a previous study from the Oygarden Group of islands that focused on ~930 Ma overgrowths on older zircon grains from orthogneiss and structurally constrained pegmatitic dykes (Kelly *et al.* 2002). Here we present U/Pb SHRIMP data for zircon grains from three Archaean orthogneiss samples and a Proterozoic pegmatite from the Oygarden Group, which reveal a tectonothermal history for the region that extends back into the Archaean. These data show considerable isotopic disturbance that is interpreted to result from modification of zircon cores during development of recrystallised zircon rims during successive thermal events. The textural zoning characteristics of zircon grains are described, and a comparison of textural zoning in zircon grains, Th–U chemistry and U–Pb ages, is used to infer the origin of particular textural morphologies and possible processes that accompanied the modification of zircon. Age data are discussed within the context of the Oygarden structural history and the regional Antarctic geochronological framework.

1. Geological setting

The Rayner Complex was originally defined by Kamenev (1972) to divide the anhydrous granulite facies rocks of the Napier Complex from those of lower metamorphic grade in western Enderby Land that contained appreciable hornblende (Sheraton *et al.* 1987; Harley & Hensen 1990; Tingey 1991). The term is now commonly applied to the Neoproterozoic mobile belt that extends from western Enderby Land to the northern Prince Charles Mountains in east Antarctica (Fig. 1; Sheraton *et al.* 1996; Carson *et al.* 2000a; Dunkley *et al.* 2003; Kelly *et al.* 2002). It forms part of a larger orogenic belt that, prior to the break-up of Gondwana, is thought to have included the Eastern Ghats Granulite Belt of India (Grew & Manton 1986; Fitzsimons 2000; Rickers *et al.* 2001), and developed as a result of convergence between eastern peninsula India and a part of east Antarctica between ~1000 and 900 Ma (Yoshida *et al.* 1996; Mezger & Cosca 1999). The Oygarden Group of islands lie in the Rayner Complex of central Kemp Land adjacent to its boundary with the Archaean Napier Complex. The Napier Complex, which forms

https://doi.org/10.1017/S0263593300001176 Published online by Cambridge University Press

Table 1 Summary of evolution of Napier and Rayner Complexes and previous geochronology

Age	Napier Complex	Age	Rayner Complex
~3800 Ma	protolith to oldest orthogneiss[1,2]		
		~3100 Ma	depleted tonalite (Edward VIII Gulf: Rb/Sr w.r. isochron)[10]
2980–2850 Ma	dominant tonalitic orthogneiss[1,2]		
2840–2820 Ma	granulite facies metamorphism[2,3]		
		2692 ± 48 Ma	felsic orthogneiss (Stillwell Hills: Rb/Sr w.r. isochron[11]
2626 ± 28 Ma	granodioritic orthogneiss[4]		
2560–2480	UHT metamorphism[4,5,6,7,8]	~2500 Ma	depleted granite and garnet gneiss (Edward VIII Gulf: Rb/Sr w.r. isochron)[10]
~2450 Ma	amphibolite-granulite facies shear zones[1,2,3,9]		
		~1600 Ma	?felsic? magmatism & metamorphism (Oygarden Group)[12]
		1100–980 Ma	intermediate & felsic magmatism (nPCMs)[13,14,15,17,18,20,23]
~1000 Ma	marginal reworking in retrograde shear zones	995–980 Ma	granulite facies metamorphism (Mawson Coast, nPCMs)[13,14,15,16,17,18,20]
		~960 Ma	charnockite (Mawson Coast, nPCMs)[16,17,21]
		940–910 Ma	granulite facies metamorphism (Kemp Land, Mawson Coast, nPCMs)[12,14,18,19,20,21]
		~900 Ma	amphibolite facies metamorphism (nPCMs)[18]
~550–500 Ma	marginal reworking in retrograde shear zones	550–500 Ma	discrete amphibolite facies mylonites (nPCMs, ?MacRobertson Land ?Kemp Land)[22], ?granulite facies reworking of western Enderby Land[7]

References: (1): Black *et al*. 1986; (2) Harley & Black, 1997; (3) Sheraton *et al*. 1987; (4) Carson *et al*. 2002a; (5) Grew, 1978; (6) Grew & Manton, 1979; (7) Shiraishi *et al*. 1997; (8) Harley, 2001; (9) Black *et al*. 1983; (10) Sheraton & Black, 1983; (11) Clarke, 1987; (12) Kelly *et al*. 2002; (13) Black *et al*. 1987; (14) Manton *et al*. 1992; (15) Kinny *et al*. 1997; (16) Young *et al*. 1997; (17) Zhao *et al*. 1997; (18) Boger *et al*. 2000; (19) Dunkley *et al*. 2003; (20) Carson *et al*. 2000a; (21) Young & Black, 1991; (22) Boger *et al*. 2002; (23) Mikhalsky *et al*. 1996.

most of the coastal exposures of Enderby Land and western Kemp Land (between 48–57°E and 66–68°S) is an Archaean craton that includes igneous precursors to orthogneiss as old as ~3800 Ma, but mostly between 2980 and 2850 Ma in age (Black *et al*. 1986; Harley & Black 1997). At least three major episodes of deformation affected the Napier Complex between ~2980 Ma and 2450 Ma (Sheraton *et al*. 1987; Harley & Black 1997). A summary of ages and events in the Napier and Rayner Complexes is provided in Table 1.

Previous isotopic work on Rayner Complex rocks exposed in Kemp Land has established that this region contains Archaean crust (Sheraton & Black 1983; Clarke 1987). Rocks as old as ~3100 Ma have been identified in Edward VIII Gulf (Rb/Sr whole rock isochron; Sheraton & Black 1983), and the area was interpreted to comprise Archaean rocks variably modified during metamorphism at ~2500 Ma (Sheraton *et al*. 1987). In addition, a 2692 ± 48 Ma Rb–Sr whole rock age for a felsic orthogneiss from the Stillwell Hills may represent the crystallisation of the igneous protolith, a metamorphic event or both (Clarke 1987). Orthogneiss exposed along the Mawson Coast, northern Prince Charles Mountains and western Enderby Land have predominantly juvenile crustal protoliths that are Proterozoic in age (Black *et al*. 1987; Young *et al*. 1997; Zhao *et al*. 1997). Peak granulite facies metamorphism and extensive felsic magmatism affected western Enderby Land, Mawson Coast and northern Prince Charles Mountains between ~995–980 Ma (Grew 1978; Manton *et al*. 1992; Kinny *et al*. 1997; Shiraishi *et al*. 1997; Dunkley 1998; Boger *et al*. 2000; Dunkley *et al*. 2003) forming the first phase of the Rayner Structural Episode (RSE; Sandiford & Wilson 1984). A second phase of metamorphism and deformation at slightly lower grades on the Mawson Coast and northern Prince Charles Mountains occurred between ~940 and 900 Ma and followed the emplacement of voluminous charnockite at ~955–985 Ma (U/Pb zircon ages; Young & Black 1991; Manton *et al*. 1992; Zhao *et al*. 1997; Dunkley 1998; Boger *et al*. 2000; Carson *et al*. 2000a; Dunkley *et al*. 2003). This second phase of deformation correlates with tectonic reworking of central and eastern Kemp Land between ~930–910 Ma, the only RSE deformation to affect that area (Kelly *et al*. 2000, 2002).

The Oygarden Group (Fig. 1) mostly exposes layered felsic to mafic orthogneiss, with subordinate pelitic, semi-pelitic and calc-silicate gneiss; all were multiply deformed at granulite facies conditions. At least five episodes of high-grade deformation (D_1 to D_5; Table 2) affected the Oygarden Group, with D_3 and D_4 representing the effects of the RSE in the area (Kelly *et al*. 2000, 2002). The most abundant unit is *layered composite orthogneiss* (*LCO*), rare components of which preserve an S_1 foliation defined by aligned leucocratic segregations (Fig. 2a). Remnants of this migmatitic S_1 are only distinguished from S_2 where locally cut by *homogeneous felsic orthogneiss* (*HFO*), which preserves evidence of an intense S_2 foliation (Fig. 2a). In all but those areas that record minimal D_2, D_3 and D_4 strain, S_1 has been transposed into parallelism with, and is indistinguishable from, later foliations. Moreover, the intensity of recrystallisation associated with D_3 and D_4 makes positive identification of S_2 difficult outside of low D_3 and D_4 strain domains.

A suite of mafic dykes that cut S_2 was intensely deformed and metamorphosed at granulite facies conditions during D_3 and D_4. The D_3 event involved high-grade ductile thrusting with an eastward transport direction, accompanied by tight to isoclinal folding. Mineral assemblages that define S_3 foliations in D_3 shear zones reflect metamorphic conditions of $P \approx 9$–11 kbar and $T \approx 800$–850°C (Kelly *et al*. 2000). Overgrowths on zircon grains in *HFO* have ages of 929 ± 12 Ma and 924 ± 17 Ma, interpreted as the age of the D_3 event (U/Pb SHRIMP ages; Kelly *et al*. 2002). A 2–3 kilometre-wide, east-trending and steeply south-dipping extensional shear zone

https://doi.org/10.1017/S0263593300001176 Published online by Cambridge University Press

Table 2 Summary of deformation events

Event	Style of event	*P–T conditions*
D_1	• migmatitic layering and layer parallel foliation	
	Intrusion of protolith to homogeneous felsic orthogneiss	
D_2	• rare F_2 isoclinal folds	(?anhydrous?)
	• transposition of S_1 and post-D_1 felsic orthogneiss into S_2	granulite facies
	Intrusion of mafic dykes (possible Amundsen Dyke correlates)	
D_{3a}	• ductile, low angle thrusting: E-trending transport axis	granulite facies
	• isoclinal recumbent folds and sheath folds: axes parallel to L_{3a}	P =10–11 kbars; T =800–850°C
D_{3b}	• upright-reclined, open-tight-isoclinal folds, E-trending axes (parallel to L_{3a} and F_{3a} axes; L_{3b} parallel to L_{3a})	
	• intense strain partitioning, strain concentrated in steeply S-dipping high strain zones parallel to F_{3b} axes	
D_4	• E–W trending, S-dipping, 2 km wide high strain zone	granulite facies
	• partial to complete transposition of D_3 structures	P =9–10 kbars; T=850°C
	• L_4 mineral rodding: steeply ESE plunging	
	• possible extensional shear sense	
	Intrusion of felsic pegmatitic dykes	
D_5	• discrete mylonite and ultramylonite zones (± pseudotachylite) general S over N directed thrust transport	amphibolite facies

N.B. Structural history summarised from Kelly *et al.* (2000).

developed during D_4; slip occurred at metamorphic conditions similar to those that accompanied D_3 (Kelly *et al.* 2000). A syn-D_4 pegmatite has been dated at 931 ± 14 Ma, within error of estimates for D_3, suggesting that D_3 and D_4 occurred as two closely spaced events (Kelly *et al.* 2002). Narrow D_5 mylonite and ultramylonite zones that cut RSE structures, which have a south over north sense of thrusting and occurred at amphibolite facies conditions, are not as yet constrained in age.

2. Sample descriptions

Samples OG615 and OG525 were taken from a domain of low D_2, D_3 and D_4 strain, therefore locally preserving intrusive relationships between *HFO* and *LCO*. Although this relationship is preserved, the area has been deformed by meso- to macroscopic D_3 deformation and all assemblages are assumed to have re-equilibrated during this event. Sample OG615 is from a felsic layer within the *LCO* that was intruded by *HFO* cutting S_1 defined by coarse-grained trails of orthopyroxene and garnet, and elongate quartz and feldspar grains. The outcrop from which the sample was taken (Fig. 2a) also contains layering defined by deformed remnants of coarse leucocratic segregations that are 1–10 cm in thickness and aligned in S_1. *LCO* does not contain S_2 or S_3 foliations at this locality. Sample OG525 is an example of *HFO* that cuts S_1 in *LCO* (sample OG615), but contains an intense S_2 gneissosity (Fig. 2a). Trails of orthopyroxene, and elongate grains of quartz, plagioclase, K-feldspar and minor ilmenite define the S_2 foliation. Sample OG473 was taken from a homogeneous felsic layer within *LCO* that is folded by an upright F_3 fold (Fig. 2b). It is similar in appearance and has a similar mineral assemblage to sample OG525, but preserves no intrusive features. It is interpreted to be *HFO* that was transposed into S_2 and deformed during D_3. Sample OG471 is from a deformed orthopyroxene-bearing pegmatite that was intruded along the axial plane of an F_3 fold (Fig. 2c) and preserves an S_3 foliation defined by perthite, antiperthite, ribbon quartz and orthopyroxene. It is interpreted to have intruded during D_3 cutting *LCO*.

3. Analytical procedure

Samples were initially crushed and zircon grains concentrated using magnetic separation and heavy liquids. The zircon grains were mounted in epoxy at the Research School of Earth Sciences, Australian National University (ANU), Canberra, along with grains of the SL13 and AS3 reference zircon. Prior to analysis by SHRIMP II at ANU, cathodoluminescence (CL) and back scattered electron (BSE) images of the sectioned grains were prepared at the Electron Microscope Unit in the School of Biological Sciences, ANU. Further BSE and CL imaging was carried out at the Department of Geology & Geophysics, University of Edinburgh. Procedures for SHRIMP analysis follow those summarised in Williams (1998, and references therein). The data were reduced according to the methods covered in detail by Williams (1998), with augmented uncertainties for the isotope ratios using the software of T. R. Ireland (see Muir *et al.* 1996). Corrections for common Pb for zircon analyses were made using the measured $^{204}Pb/^{206}Pb$ ratio, and the common Pb composition of Broken Hill lead ore. The Pb/U ratios were normalised relative to a value of 0·1859 for the $^{206}Pb/^{238}U$ ratio of the AS3 reference zircon grains (1099·1 Ma; Paces & Miller 1993). For analyses relative to the SL13 reference zircon, a $^{206}Pb/^{238}U$ ratio of 0·0928 was used (572·2 Ma; Claoué-Long *et al.* 1995). Uncertainties quoted in tables and in the text for *individual analyses* (ratios and ages) and *error ellipses* on standard Wetherill concordia diagrams are at the 1σ level. All uncertainties in calculated *group* ages are reported at 95% confidence limits; plots and age calculations have been made using ISOPLOT/EX (Ludwig 1999).

4. Results

4.1. Texturally defined zircon types

Under transmitted light, most zircon grains are colourless; rare inclusions are usually confined to the cores of grains. Under Scanning Electron Microscope (SEM), the zircon grains show complex internal textures reflecting repeated growth and recrystallisation during metamorphism. Four core and two rim

https://doi.org/10.1017/S0263593300001176 Published online by Cambridge University Press

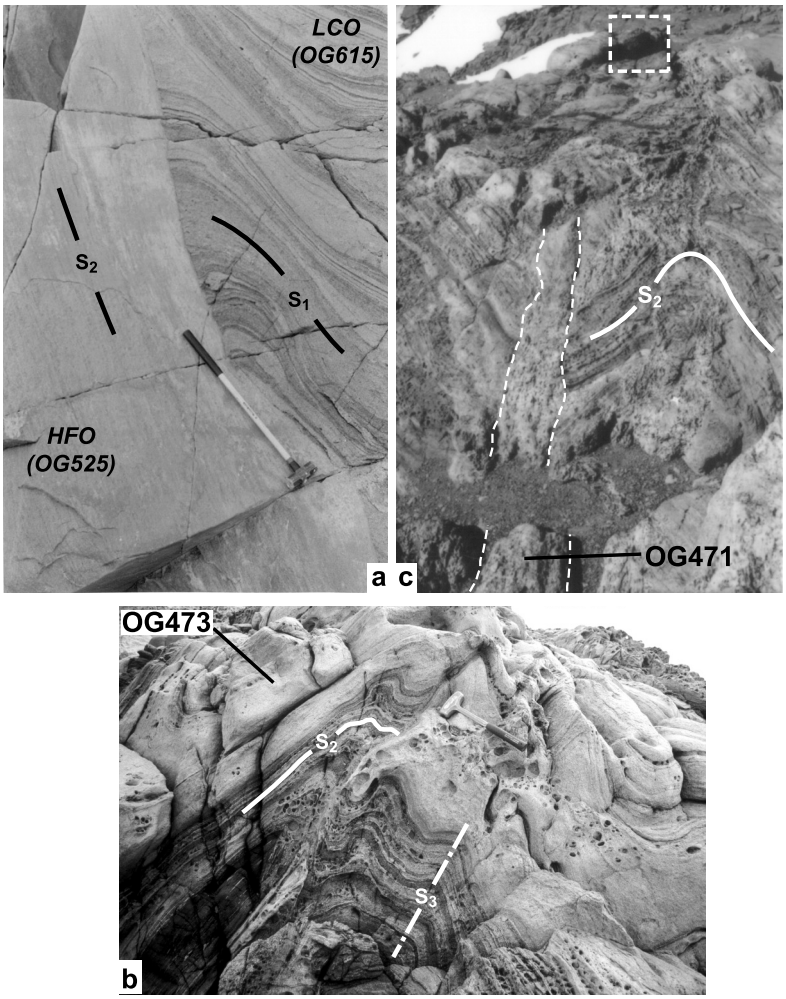

Figure 2 (a) Outcrop photograph showing an igneous contact between *layered composite orthogneiss* and *homogeneous felsic orthogneiss*, and the structural context and locations of samples OG615 and OG525. S_1 in the *LCO* is defined in part by layering, aligned leucocratic segregations and trails of coarse-grained minerals. Note the isoclinally folded leucocratic layer in the *LCO* adjacent to the contact with *HFO*. No evidence for a folded gneissosity was evident thereby providing no solid evidence for deformation event prior to that identified in the text as D_1. (hammer is approx. 1 m in length). (b) Outcrop photograph showing the structural context and location of sample OG473. S_2 layering across the outcrop is deformed by upright F_3 folds and offset along a narrow shear zone parallel to the S_3 axial surface. The sample was taken from the broad felsic layer. (hammer is approx. 40 cm in length). (c) Outcrop photograph showing the structural context and location of sample OG471. The pegmatitic dyke intruded along the axial plane of a F_{3b} fold, cutting S_2 and containing S_3. (a camera bag for scale sits inside the white dashed box).

types have been identified based on visual characteristics and are summarised in Table 3. Each type is not assumed to have formed during the same event in each sample, although this may be the case for some. Not all core and rim 'Types' occur in each sample and each 'Type' displays minor variations within and between samples. This variation is discussed below.

Type C1 cores are weakly to moderately luminescent and commonly preserve a well-defined oscillatory zoning (Fig. 3a, b). Most C1 cores are elongate (e.g. OG525; Fig. 3b), but may be stubby with rounded terminations (OG473). C1 cores are interpreted to be igneous zircon grains or grain relics. Many C1 cores are rounded with oscillatory zoning truncated by outer growth zones (outer cores or rims), suggesting many, if not all, C1 cores are inherited xenocrysts. Samples OG525 and OG473 also contain moderately luminescent zircon cores that have patchy oscillatory zoning or blurred boundaries between oscillatory zones (Fig. 3c). In some cases only a very faint, ghost-like relic of a circular zoning pattern is preserved (Fig. 3d), which may reflect the partial recrystallisation or annealing of pre-existing structures.

Type C2 cores are moderately luminescent and are commonly homogeneous when viewed using CL and BSE (Fig. 3e, f, g). Some cores preserve faint, patchy zoning (Fig. 3h). C2 cores are commonly stubby or round in shape and are interpreted to have formed during metamorphism, either through growth or recrystallisation of pre-existing zircon.

Type C3 cores contain more diverse internal textural zoning compared with C1 or C2 cores. These cores are weakly to moderately luminescent and within single grains preserve a combination of radial and irregular sector zoning, 'fir-tree' sector zoning and planar growth banding (OG615; Fig. 3i, j). This type of mixed zoning is interpreted to result from fluctuating crystal growth rates (Vavra *et al.* 1996, 1999) and is commonly observed in zircon that has crystallised from anatectic melt or grown in the presence of partial melt (Vavra *et al.* 1996, 1999; Rubatto *et al.* 1998; Schaltegger *et al.* 1999; Kelly *et al.* 2002).

Type C4 cores preserve broad concentric zoning and are weakly to moderately luminescent (Fig. 3k). They are stubby to elongate in shape and are interpreted to have formed or modified during metamorphism, possibly in the presence of melt.

Type R1 rims are moderate to very highly luminescent, and commonly have a 'bleached' appearance. They are broadly

https://doi.org/10.1017/S0263593300001176 Published online by Cambridge University Press

Table 3 Summary of zircon core and rim morphologies interpreted from SEM imaging; minor variations within samples are discussed in the text

Zircon type	Description	CL response	Samples	Interpretation
C1	Oscillatory zoning; may be patchy	Low to moderate	OG615, OG525, OG473, OG471	magmatic, commonly partially recrystallised or modified
C2	Homogeneous; may be patchy in some samples; rounded and irregular shapes in OG471	Moderate	OG525, OG473, OG471	metamorphic growth and/or highly modified magmatic
C3	Radial & irregular sector zoning, 'fir-tree' sector zoning, and planar growth banding	Low to moderate	OG613	growth from, or in the presence of melt at high temperatures
C4	broad concentric zoning	Moderate to low	OG473	metamorphic recrystallisation/growth
R1	Homogeneous with some patchy or weakly developed concentric zoning	Moderate to high	OG525, OG473, OG471	modification of pre-existing zircon during metamorphism
R2	Homogeneous, variable in width between samples	Moderate to low	OG615, OG473	metamorphic growth

homogeneous (Fig. 3e), but may preserve patchy (Fig. 3l) or concentric zoning (Fig. 3m, n). R1 rims can be quite thick (up to 100 μm: Fig. 3d) and may be continuous or discontinuous (Fig. 3h, n). These rims commonly embay cores along curved and undulating boundaries (Fig. 3d, h, l, n) or may penetrate the core in deep embayments (Fig. 3o, p) or along 'sharp' fronts (Fig. 3f). Some boundaries between cores and rims are straight and appear to follow previous structures or crystallographic faces (Fig. 3g). Ghost structures may also be preserved, which pass between the core and rim (Fig. 3l). Textures similar to these have been described elsewhere and interpreted to have formed by modification of pre-existing zircon during metamorphism (Schaltegger *et al.* 1999; Hoskin & Black 2000).

Type R2 rims are commonly homogeneous, but may preserve concentric or patchy zoning. They differ from R1 rims by being weakly luminescent (e.g. Fig. 3h, l, m), but this may be moderate in some samples, possibly suggesting some cross-over between the classification of R1 and R2 rims (e.g. R1 rims in Fig. 3p). They can be thick (e.g. OG615; Fig. 3a, i, j) or be quite thin and discontinuous (Fig. 3h, l), and are interpreted to have formed during growth of new metamorphic zircon.

4.2. U/Pb age results

The U–Pb data from all samples show a high degree of normal and reverse discordance (plotting below and above concordia, respectively in a Wetherill concordia plot; e.g. Fig. 4). A number of possible explanations have been made to account for reverse discordance in SHRIMP analyses, including matrix dependent sputtering and ionisation effects (McLaren *et al.* 1994). For example, the damaged zircon lattice in metamict zircon can lead to enhanced secondary ion yield of U over Pb, such that areas with different microstructure may produce different isotope concentrations and plot as reversely discordant data (McLaren *et al.* 1994; Black *et al.* 1986). Alternatively, the sputtering characteristics of zircon with a high abundance of labile Pb can also cause reverse discordance (Wiedenbeck 1995). Low common Pb, similar Zr_2O^+ emission of standard and unknown zircons, and a correlation between Pb/U and $^{207}Pb/^{206}Pb$ ratios, was interpreted to be possible evidence against reverse discordance in zircons being a result of analytical effects (Harley & Black 1997). These and others authors suggested diffusion of Pb from U-rich and metamict zones to more U-poor and pristine zones as driving this reverse discordance (Harley & Black 1997; Williams *et al.* 1984; Mattinson *et al.* 1996). Alternatively, geological causes of reverse discordance may be the result of localised regions of U loss relative to Pb (Kinny 1987; Harrison *et al.* 1987).

In the Oygarden zircon grains, which display a large degree of both normal and reverse discordance, significant isotopic mobility and disturbance during their evolution is evident. However, it is difficult to attribute a specific cause to reverse discordance. In some samples reverse discordance appears to be more dominant in particular morphologies. For example, the majority of C2 cores from sample OG525 zircons are reversely discordant. These grains are all low in U (C2 cores and R1 rims are <102 ppm in that sample) and are therefore not likely to have suffered intense amorphisation of their lattice through metamictisation. Differential sputtering of U and Pb is therefore not considered a likely analytical effect in this case. Reversely discordant data in all samples also show a correlation between Pb/U and $^{207}Pb/^{206}Pb$, have low common Pb and show no correlation between $^{204}Pb/^{206}Pb$ and $^{207}Pb/^{206}Pb$. Discordance is therefore not likely due to labile Pb in the zircon (Wiedenbeck 1995; Harley & Black 1997).

Zircon grains from samples OG525 and OG473 presented in this paper were analysed during two analytical sessions a year apart. In both these sessions all data from standard zircon analyses were normal, showing no evidence for instrument malfunction. Moreover, zircon grains from a third sample, collected from the same location as OG525 four years after the original, and analysed in a separate zircon mount, produced similar results to the early analytical session and new analyses on the original grain mount. During this analytical session, it was noted that the concentration of U and Pb isotopes were varying over sub-micron scales during ion probe ablation of the zircon grains (N. Kelly, unpublished data). It is therefore considered highly likely that the reverse discordance observed in the Oygarden zircon grains is not an analytical problem associated with SHRIMP analysis, but a true geological phenomenon, probably due to the migration of U and Pb in the zircon lattice during metamorphism, driven by processes that are as yet not fully understood. The following interpretation of discordant data is made in light of this.

OG615 – pre-D_1 felsic orthogneiss (location: 66°57·9′S, 057°32·2′E)

Zircon grains from this sample are commonly stubby to elongate in shape, and between 100 and 250 μm in size. Internal textural morphologies are predominantly C3 cores with R2 rims that are up to 50 μm in thickness (Fig. 3i), and less abundant C1 cores (Fig 3j). Twenty-nine analyses were

https://doi.org/10.1017/S0263593300001176 Published online by Cambridge University Press

made from 21 zircon grains in this sample. Th & U chemistry for each zircon type do not show consistent trends, with compositions typically overlapping (Fig. 5a), although R2 rims tend to have lower Th/U ratios (0·12–0·31) than the C3 cores on which they occur (0·21–1·09; Table 4a). Many analyses are normally and reversely discordant, consistent with isotopic mobility within the zircon grains. One analysis (12·1; Table 4a) was not included in Figure 4 due to extreme reverse discordance. Most remaining data lie broadly within a polygon defined by four concordant ages (~3650 Ma, 2400 Ma, 1600 Ma and 930 Ma; Fig. 4). These ages are recorded as concordant clusters of data in this and other samples. The youngest age, ~930 Ma, is interpreted to represent the timing of metamorphism that accompanied the RSE in the Oygarden Group (Kelly *et al*. 2002).

The Wetherill concordia diagram for OG615 (Fig. 4) shows a main cluster of data at ~3650 Ma, with scatter along and below the concordia curve down to Neoproterozoic ages. Only a single oscillatory zoned (C1) zircon grain was located (core to grain 16, Fig. 3a; $^{207}Pb/^{206}Pb$ age = 3612 ± 32 Ma). However, this core may be an inherited xenocryst and is also younger than the oldest concordant analysis of a C3 core ($^{207}Pb/^{206}Pb$ age = 3655 ± 15 Ma; analysis 4·1), therefore the protolith to the orthogneiss is most likely older than ~3655 Ma. Internal textural zoning in C3 cores reflects crystallisation of zircon during a high-grade thermal event that was accompanied by partial melting, consistent with the development of the leucocratic segregations in this rock. From this oldest concordant age, other data are scattered along the concordia curve to 3469 ± 13 Ma (analysis 13·2; $^{207}Pb/^{206}Pb$ age), which may reflect the affects of partial to complete resetting of isotopic ratios at this time. Amongst the remaining data, two concordant analyses from C3 cores have $^{207}Pb/^{206}Pb$ ages of 2427 ± 13 Ma and 2384 ± 8 Ma (22·1, 14·2 respectively). It is not clear if these cores reflect new growth or recrystallisation of zircon at this time. The complex discordance in the data, where lines through different populations of data intersect and no clear lines of Pb-loss can be isolated to a single period of isotopic disturbance, is interpreted to reflect the effect(s) of one (or more) periods of isotopic mobilisation.

OG525 – post-D_1, pre-D_2 felsic orthogneiss (location: 66°57·9′ S, 057°32·2′ E)

Zircon grains from OG525 are a mix of elongate and stubby or round grains. The grains show complex internal textural zoning comprising C1 and C2 cores and R1 rims. Forty-eight analyses from 31 zircon grains include a number of analyses with either normal or reverse discordance. Th and U chemistries show wide variations within and between zircon types and have no consistent or systematic patterns (Fig. 5b), although R1 rims typically have lower U and Th than the cores they occur on (Table 4b). Many C1 cores are well rounded and have oscillatory zoning that is truncated by overgrowths (Fig. 3b), so they are interpreted to be inherited xenocrysts. Four analyses of these grains have ages of ~3600 Ma (Group 1: Table 4b). Nine analyses of R1 rims that form the ~930 Ma population (Group 4) have a mean $^{206}Pb/^{238}U$ age of 924 ± 17 Ma (Kelly *et al*. 2002).

Most remaining data lie broadly within a polygon on the Wetherill concordia diagram defined by major clusters of data at ~2750 Ma, 2400 Ma and 930 Ma (Fig. 6). Two clear lines of discordant data, comprising Group 2 and Group 3 (Table 4b), project towards ~930 Ma. From Group 2 data (25 analyses), six have been rejected (4·1, 9·1, 11·2, 22·2, 28·1, 29·1) for being extremely reverse discordant (Fig. 6a). These analyses were from C2 cores and have $^{207}Pb/^{206}Pb$ ages that are between 2635 and 2762 Ma. A further three analyses were rejected for clearly lying off the regression line (1·2, 5·2, 19·1). The remaining 17 analyses are predominantly from R1 rims and some C2 cores. The data include one concordant analysis, taken from a R1 rim (analysis 10·2), that has a $^{207}Pb/^{206}Pb$ age of 2733 ± 23 Ma. The remaining data define a Pb-loss mixing line that projects towards ~930 Ma so a regression through this data was anchored at ~924 Ma, the average age of R1 rims that define the lower end of the Pb-mixing line (Fig. 6b, inset). This regression has an upper intercept age of 2781 +44/-45 Ma (MSWD = 1·4). The geological meaning of this upper intercept is not conclusive, but in the absence of magmatic zircon grains, this age reflects the minimum age of the protolith to this orthogneiss. However, the discordance in data indicates that these grains suffered intense recrystallisation and Pb-loss at ~930–910 Ma.

The second group of data (Group 3: nine analyses) have $^{207}Pb/^{206}Pb$ ages that mostly cluster around ~2400 Ma. Two analyses (3·2, 6·1) are from cores that preserve faint concentric zoning and have Th/U ratios that are much higher than the rest of Group 3 analyses (>1·5 compared with <0·50). These zircon grains may reflect older magmatic zircon, recrystallised at ~2400 Ma. The remaining Group 3 data are from C2 cores and R1 rims and define a Pb-loss mixing line that projects toward ~930 Ma. One analysis was rejected (7·2) for lying off the chord, and a regression through the remaining data, anchored at ~924 Ma, has an upper intercept with the concordia curve at 2319 +46/-47 Ma (MSWD = 1·4). This upper intercept age is interpreted to reflect the minimum age of metamorphic zircon that was subsequently affected by metamorphism at ~930–910 Ma.

OG473 – post-D_1, pre-D_2 felsic orthogneiss (location: 66°57·2′ S, 057°29·0′ E)

Zircon grains from OG473 are complexly zoned and comprise C1 and C2 cores, R1 and R2 rims. Forty analyses were made from 25 zircon grains, most of which show evidence for isotopic disturbance (Fig. 7). Of the forty analyses, three (1·2, 7·1, 8·1: Group 1; Table 4c) are from C1 cores, two of which have $^{207}Pb/^{206}Pb$ ages of ~3500 Ma. These cores are rounded and oscillatory zoning is truncated by overgrowths, so they are interpreted to be inherited zircon xenocrysts. The remaining data in this sample show complex isotope mixing, with only one clear data population defined at ~930 Ma (Group 3). This Group comprises eight analyses from R2 rims that have a mean $^{207}Pb/^{206}Pb$ age of 929 ± 10 Ma (Kelly *et al.* 2002). Analyses from this population of R2 rims have Th and U chemistries that are distinct from other R2 rims and zircon types (Fig. 5c), and therefore reflect a separate period of zircon growth. Other zircon types show a wide variation in compositions and no systematic Th/U ratio patterns.

Within the remaining Late Archaean and Proterozoic data (Group 2) no clear Pb-loss mixing lines are apparent, but the discordance in data generally trends towards ~930 Ma (Fig. 7b). Two analyses from C1 cores with 'fuzzy' zoning patterns yielded $^{207}Pb/^{206}Pb$ ages of 2713 ± 11 Ma and 2785 ± 33 Ma (9·1 and 10·1 respectively). However, the bulk of the data in Group 2 are from C2 cores *and* R1 rims. Near to concordant analyses from this population have $^{207}Pb/^{206}Pb$ ages that are spread between 2750 and 2350 Ma, with the youngest concordant analysis at ~2518 Ma (27·1). There is also a spread of significantly discordant data with $^{207}Pb/^{206}Pb$ ages that range down to ~1700 Ma, and have Pb-loss mixing lines that suggest that they crystallised before ~2400 Ma.

The complexity in Late Archaean and Palaeoproterozoic data from this sample is consistent with appreciable isotopic mobility and Pb-loss. The spread of $^{207}Pb/^{206}Pb$ ages between 2840 and 2400 Ma from C2 zircon cores and R1 rims may be interpreted in a number of ways. The oldest analysis in this group (1·1) is taken from a R1 rim on a C1 core. As this rim

displays reverse discordance, the meaning of this age is unclear. This age may reflect the timing of rim development at ~2840 Ma, or if only partial resetting of the core age has occurred, an age that is intermediate between the core age and the age of rim development. If the former explanation is accepted, the ~2840 Ma age of R1 rims also a minimum age on the development of C2 cores. If the latter scenario is accepted, the ~2840 Ma age is geologically meaningless, with younger, more concordant ages placing constraints on R1 rim, and therefore C2 core development. In the absence of more convincing information the ~2840 Ma age is taken to be a possible minimum age for the protolith to OG473.

As the configuration of the Wetherill diagram is such that data from zircon that suffered Pb-loss within 500 Ma of crystallisation will track near to, or along, concordia (Mezger & Krogstad 1997), the scatter of concordant and slightly discordant ages between 2750 and 2400 Ma could have been caused by thermally-induced disturbance of zircon grains that

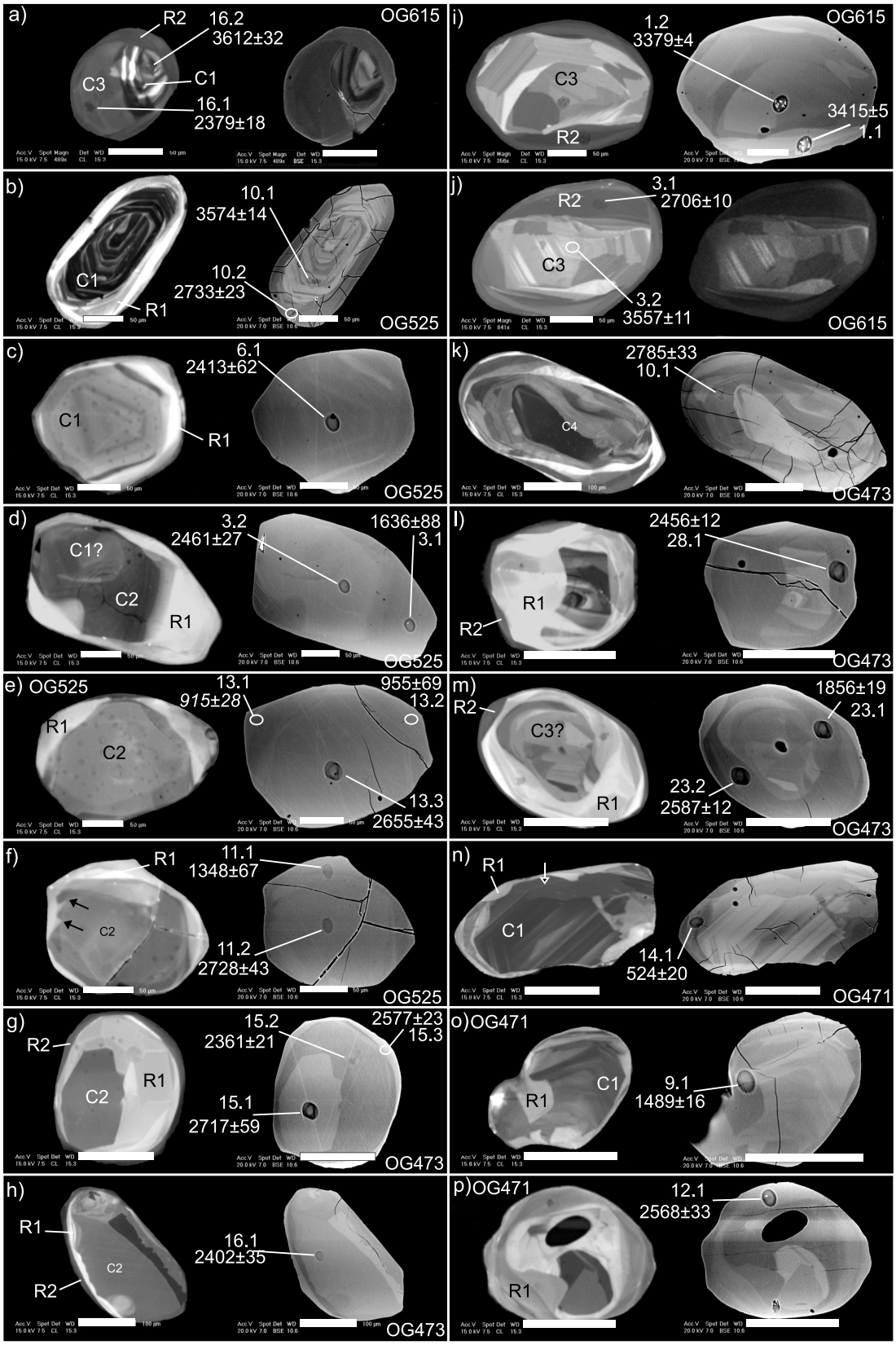

https://doi.org/10.1017/S0263593300001176 Published online by Cambridge University Press

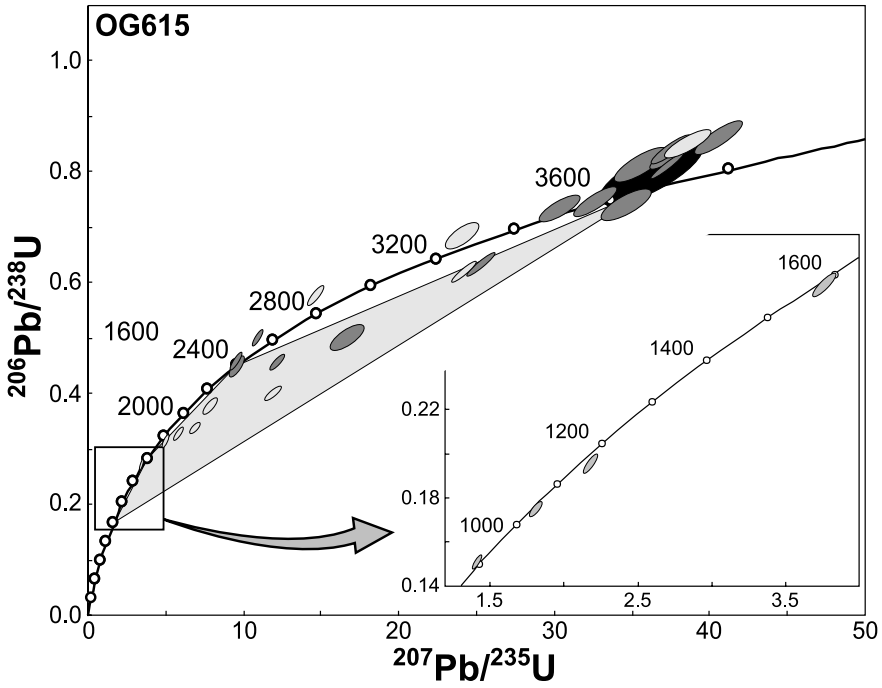

Figure 4 *Top*: Standard Wetherill concordia diagram showing the distribution of U–Pb data from sample OG615. The data show a dominant cluster at ~3650 Ma, moderate reverse discordance and Pb-loss toward a Proterozoic age. The shaded area indicates the probable scope of Pb-loss mixing lines inferred from known metamorphic zircon ages in this and other samples. Shaded symbols: (black) C1 core; (dark grey) C3 cores; (light grey) R2 rims. *Inset*: four analyses scattered between 1600 and 900 Ma.

originally formed at or before 2840 Ma. The timing of this disturbance could be reflected by a concordant R1 rim analysis at ~2518 Ma (27·1) or younger, slightly discordant analyses at or around ~2400 Ma. Further metamorphism may be inferred to have occurred at ~1600 (R1 & R2 rims: 6·1, 12·1, 12·2) and there is clear evidence for metamorphism at ~930 Ma (Kelly *et al*. 2002). These multiple, overprinting events would have caused further isotopic disturbance, creating the complex data array.

OG471 – syn-D_3 felsic pegmatite (location: 66°56·6′S, 057°33·6′E)

Twenty-four analyses were made from 20 zircon grains. Of these, 16 analyses were from grains that were interpreted to be inherited and were used to establish inheritance patterns in the pegmatite. Consistent with most zircon grains from other samples, Th and U chemistries of the zircon types represented in this sample have no systematic patterns. Although R1 rims typically have lower U compared with the cores they occur on. Analyses have been grouped into three populations. Group 1 is composed of ten analyses that have $^{207}Pb/^{206}Pb$ ages that range between 2600 and 2000 Ma (Table 4d; Fig. 8). These analyses were taken from C1 and C2 cores, and R1 rims. Data acquired from C1 cores (five analyses) form an array along concordia between 2474 ± 7 Ma and 2028 ± 10 Ma. Analyses from C2 cores (2) and R1 rims (3) have an upper age limit defined by a concordant analysis of a R1 rim at 2568 ± 33 Ma (12·1). The remaining analyses are scattered around ~2400 Ma and may be consistent with metamorphic growth or modification of zircon by this time. Group 2 comprises six analyses that were taken from R1 rims and have $^{207}Pb/^{206}Pb$ ages that mostly cluster around 1600 Ma. Group 3 comprises eight analyses from R1 rims that are interpreted to have formed *in-situ*, and suggest that the pegmatite crystallised before ~870 Ma (Kelly *et al*. 2002).

Figure 3 Back Scattered Electron and Cathodoluminescence images of selected zircons from samples OG615, OG525, OG473 and OG471; $^{207}Pb/^{206}Pb$ age are quoted with 1σ errors and all scale bars are 50 μm. (a) Type C1 inner core that preserves oscillatory zoning, outer, weakly luminescent Type C3 core with patchy sector zoning, and a homogeneous R2 rim that truncates zoning in the oscillatory zoned core. (b) Inherited zircon with an oscillatory zoned Type C1 core. The core is surrounded by a patchy, concentrically zoned, highly luminescent Type R1 rim. (c) Oscillatory zoned Type C1 core (sectioned normal to the C-axis) where zoning has been 'blurred' through partial recrystallisation, surrounded by a discontinuous 'bleached' highly luminescent Type R1 rim. (d) Moderately luminescent core with faint concentric zoning that may represent recrystallised magmatic zoning, embayed and surrounded by a 'bleached' highly luminescent Type R1 rim that deeply embays the core on one side. (e) Homogeneous 'metamorphic' Type C2 core with 'bleached' highly luminescent R1 rims. (f) Moderately luminescent Type C2 core surrounded by a 'bleached' highly luminescent Type R1 rim. On the left of the zircon rain, sharp fronts embay the core from the rim, as indicated by arrows. (g) Homogeneous moderately luminescent Type C2 core surrounded by a thick highly luminescent outer core (Type R1) and a thin outer weakly luminescent Type R2 rim. (h) Complexly zoned zircon that preserves a band of weakly luminescent zircon that has irregular boundaries within the surrounding homogeneous core. The core is rimmed by a thin and discontinuous, highly luminescent layer that embays the core along multiple, curved fronts. (i) & (j) show large Type C3 cores that preserve complex zoning patterns including sector, concentric, planar growth banding and homogeneous zoning. These are rimmed by homogeneous and faint concentrically zoned Type R2 zircon. (k) Moderately luminescent Type C4 core with broad circular zoning. (l) Complexly zoned, weakly to moderately luminescent core with irregular zoning. The core is surrounded by a thick, 'bleached' highly luminescent Type R1 rim that embays the core along broad, curved boundaries that suggest recrystallisation related to diffusion or fluid activity. (m) Possible Type C3 core with patchy zoning that is surrounded and embayed by highly luminescent Type R1 rims. A thin and discontinuous, moderately luminescent Type R2 outer rim also occurs. (n) Inherited, weakly to moderately luminescent Type C1 core that preserves part oscillatory zoning. The core is embayed along curved boundaries by a highly luminescent Type R1 rim. (o) Moderately luminescent core with concentric, faceted zoning that may reflect partially recrystallised magmatic zircon. The core is deeply embayed by a thin, moderately to highly luminescent Type R1 rim. (p) Zircon with multiple core zones that may reflect inheritance or multiple episodes of recrystallisation. The core is surrounded and embayed by a moderately luminescent Type R1 rim.

https://doi.org/10.1017/S0263593300001176 Published online by Cambridge University Press

Table 4a–d Summary of SHRIMP U-Pb zircon results for samples OG615, OG525, OG473, OG471

	Analysis no.	Zircon type	U (ppm)	Th (ppm)	Th/U	Pb* (ppm)	204 / ppb	$^{204}Pb/^{206}Pb$	f_{206} %	Radiogenic rates $^{206}Pb/^{238}U$	±	$^{207}Pb/^{235}U$	±	$^{207}Pb/^{206}Pb$	±	Ages (in Ma) $^{206}Pb/^{238}U$	±	$^{207}Pb/^{235}U$	±	$^{207}Pb/^{206}Pb$	±	Conc.%
(a) Sample OG615																						
	1·1	R2	763	93	0·12	366	2	0·000006	0·007	0·623	0·007	24·31	0·29	0·2829	0·0007	3123	29	3281	12	3379	4	92
	1·2	C3	219	60	0·27	111	1	0·000011	0·013	0·636	0·008	25·36	0·34	0·2894	0·0010	3172	32	3322	13	3415	5	93
	2·1	R2	681	134	0·20	204	2	0·000010	0·011	0·404	0·005	12·15	0·18	0·2180	0·0017	2188	22	2616	14	2966	13	74
	2·2	C3	174	99	0·57	122	1	0·000011	0·013	0·812	0·013	35·49	0·68	0·3170	0·0029	3832	45	3652	19	3555	14	108
	3·1	R2	1053	161	0·15	441	3	0·000008	0·011	0·581	0·006	14·90	0·19	0·1859	0·0011	2954	26	2809	12	2706	10	109
	3·2	C3	221	95	0·43	139	2	0·000016	0·019	0·746	0·010	32·65	0·53	0·3174	0·0022	3593	38	3570	16	3557	11	101
	4·1	C3	236	89	0·38	171	3	0·000026	0·03	0·742	0·010	34·62	0·63	0·3383	0·0034	3579	39	3628	18	3655	15	98
	5·1	C3	1388	439	0·32	1082	5	0·000006	0·007	0·811	0·009	37·28	0·40	0·3333	0·0004	3829	31	3701	11	3632	2	105
	5·2	R2	706	216	0·31	301	2	0·000008	0·011	0·505	0·006	11·17	0·13	0·1605	0·0005	2634	24	2537	11	2461	5	107
	6·1	C3	779	167	0·21	347	3	0·000010	0·011	0·506	0·009	16·86	0·41	0·2415	0·0035	2641	39	2927	24	3130	23	84
	7·1	C3	462	125	0·27	182	0	—	<0·01	0·461	0·005	12·41	0·16	0·1952	0·0008	2444	24	2636	12	2787	7	88
	8·1	C3	253	135	0·53	218	1	0·000008	0·009	0·862	0·011	40·41	0·61	0·3399	0·0021	4008	39	3781	15	3662	9	109
	9·1	R2	856	200	0·23	99	1	0·000015	0·025	0·150	0·002	1·403	0·019	0·0679	0·0004	900	10	890	8	866	11	104
	10·1	R2	928	124	0·13	728	0	0·000001	0·001	0·851	0·010	38·53	0·60	0·3286	0·0026	3968	36	3734	15	3610	12	110
	11·1	R2	783	181	0·23	212	1	0·000008	0·011	0·333	0·004	6·122	0·097	0·1334	0·0010	1852	21	1993	14	2143	13	86
	12·1	C3	165	78	0·47	201	4	0·000026	0·03	1·229	0·021	59·49	1·06	0·3511	0·0012	5167	61	4166	18	3712	5	139
	13·1	R2	565	134	0·24	77	3	0·000038	0·065	0·174	0·002	1·793	0·025	0·0746	0·0005	1036	11	1043	9	1057	13	98
	13·2	C3	248	148	0·60	181	4	0·000030	0·035	0·736	0·010	30·40	0·51	0·2998	0·0026	3554	37	3500	17	3469	13	102
	14·1	R2	519	122	0·24	114	1	0·000010	0·015	0·277	0·003	3·747	0·052	0·0980	0·0006	1578	17	1581	11	1586	11	100
	14·2	C3	1025	318	0·31	400	0	—	<0·01	0·464	0·005	9·82	0·13	0·1534	0·0007	2459	24	2418	12	2384	8	103
	15·1	C3	460	222	0·48	380	3	0·000011	0·012	0·841	0·010	37·54	0·50	0·3237	0·0012	3934	36	3708	13	3588	6	110
	16·1	R2	513	154	0·30	166	2	0·000014	0·019	0·384	0·006	8·11	0·15	0·1530	0·0016	2096	26	2243	17	2379	18	88
	16·2	C1	891	44	0·05	646	3	0·000007	0·008	0·798	0·023	36·20	1·34	0·3289	0·0067	3782	82	3672	37	3612	32	105
	17·1	R2	984	140	0·14	592	2	0·000005	0·006	0·687	0·009	24·27	0·43	0·2563	0·0028	3370	34	3279	18	3224	17	105
	18·1	C3	244	265	1·09	223	1	0·000010	0·011	0·833	0·011	37·58	0·55	0·3271	0·0020	3907	37	3709	15	3604	9	108
	19·1	R2	904	276	0·31	237	0	—	<0·01	0·320	0·003	5·390	0·077	0·1223	0·0010	1789	17	1883	12	1989	14	90
	20·1	R2	765	201	0·26	219	1	0·000005	0·008	0·345	0·004	7·22	0·12	0·1518	0·0016	1910	20	2139	16	2367	19	81
	21·1	R2	785	183	0·23	119	1	0·000014	0·02	0·195	0·003	2·164	0·030	0·0804	0·0004	1149	14	1170	10	1207	9	95
	22·1	C3	638	180	0·28	243	1	0·000006	0·008	0·455	0·007	9·88	0·17	0·1573	0·0012	2419	30	2423	16	2427	13	100
(b) Sample OG525																						
Gr1	1·1	C1	8	5	0·56	16	0	0·000022	<0·01					0·3411	0·0036					3668	16	
	2·1	C1	233	73	0·32	147	2	0·000019	0·022	0·7631	0·0095	34·36	0·53	0·3266	0·0026	3655	35	3620	15	3601	12	102
	9·2	C1	303	120	0·40	224	2	0·000011	0·012	0·867	0·011	42·43	0·63	0·3551	0·0020	4024	39	3829	15	3729	8	108
	10·1	C1	669	305	0·46	402	3	0·000010	0·012	0·710	0·011	31·42	0·59	0·3208	0·0030	3459	41	3532	19	3574	14	97
Gr 2	1·2	C1	74	53	0·72	16	3	0·000280	0·324	0·2636	0·0082	6·49	0·52	0·178	0·013	1508	42	2044	74	2639	123	57
	2·2	R1	33	57	1·74	10	3	0·000446	0·618	0·323	0·012	7·53	0·40	0·1690	0·0056	1805	58	2176	48	2547	57	71
	3·1	R1	25	10	0·40	3	2	0·000841	1·164	0·1901	0·0050	2·64	0·15	0·1006	0·0046	1122	27	1311	42	1636	88	69
	4·1	C2	42	65	1·54	34	5	0·000227	0·315	0·823	0·017	21·08	0·50	0·1857	0·0018	3872	60	3142	23	2704	16	143
	5·2	R1	31	9	0·28	5	2	0·000480	0·765	0·237	0·013	3·08	0·38	0·0940	0·0099	1373	69	1427	100	1508	212	91
	7·1	R1	14	5	0·35	5	3	0·000753	1·043	0·429	0·015	10·69	0·66	0·1806	0·0086	2303	67	2497	59	2658	81	87
	9·1	C1	43	23	0·53	21	1	0·000085	0·118	0·659	0·018	16·19	0·53	0·1780	0·0026	3265	70	2888	32	2635	24	124
	10·2	R1	102	68	0·67	43	3	0·000097	0·109	0·5248	0·0083	13·67	0·31	0·1889	0·0026	2720	35	2727	21	2733	23	100
	11·1	R1	36	17	0·46	4	1	0·000166	0·284	0·1658	0·0046	1·98	0·09	0·0864	0·0030	989	26	1107	32	1348	67	73
	11·2	C2	69	74	1·08	70	1	0·000016	0·022	1·169	0·025	30·35	1·07	0·1883	0·0048	4990	74	3498	35	2728	43	183
	13·3	C2	32	21	0·67	14	3	0·000336	0·456	0·464	0·015	11·53	0·50	0·1802	0·0046	2457	67	2567	42	2655	43	93
	14·1	R1	42	29	0·68	12	2	0·000172	0·239	0·374	0·016	8·91	0·47	0·1727	0·0047	2048	73	2329	49	2584	46	79
	16·1	R1	31	2	0·07	10	3	0·000289	0·397	0·483	0·024	12·03	0·81	0·1807	0·0073	2541	104	2607	65	2659	68	96
	17·1	R1	37	13	0·35	6	3	0·000507	0·702	0·2286	0·0089	3·94	0·59	0·125	0·018	1327	47	1623	130	2031	272	65
	18·1	R1	18	3	0·15	5	2	0·000448	0·608	0·332	0·016	8·38	0·51	0·1830	0·0061	1850	76	2274	57	2680	56	69
	19·1	R1	7	2	0·36	1	3	0·003331	5·572	0·192	0·024	4·71	1·14	0·178	0·034	1133	131	1770	226	2634	362	43
	21·1	R1	49	33	0·67	12	2	0·000264	0·358	0·2644	0·0085	5·55	0·26	0·1524	0·0045	1512	43	1909	41	2373	51	64
	22·1	R1	19	7	0·37	4	2	0·000563	0·765	0·238	0·011	4·37	0·31	0·1332	0·0067	1376	57	1707	61	2141	90	64
	22·2	C2	47	10	0·20	45	2	0·000047	0·064	1·121	0·030	28·29	1·09	0·1830	0·0044	4847	93	3429	38	2681	40	181
	24·1	R1	41	13	0·32	6	3	0·000703	1·177	0·1769	0·0043	2·06	0·10	0·0844	0·0035	1050	23	1135	35	1302	82	81
	27·1	R1	18	15	0·83	5	2	0·000450	0·611	0·277	0·015	5·66	0·49	0·1482	0·0092	1577	74	1925	77	2325	110	68
	28·1	C2	64	33	0·52	78	1	0·000022	0·029	1·341	0·036	34·54	1·36	0·1869	0·0048	5482	101	3625	40	2715	43	202
	28·2	R1	38	15	0·41	5	4	0·000804	1·345	0·1721	0·0039	2·23	0·13	0·0938	0·0047	1024	21	1189	41	1503	97	68
	29·1	C2	76	78	1·02	51	3	0·000075	0·101	0·688	0·016	18·25	0·76	0·1923	0·0060	3375	62	3003	41	2762	52	122
	30·2	C1	32	49	1·56	8	0	0·000010	0·014	0·2399	0·0078	4·65	0·19	0·1406	0·0030	1386	41	1758	35	2234	38	62
	31·1	C2	40	51	1·26	9	1	0·000204	0·278	0·2232	0·0086	3·55	0·20	0·1153	0·0043	1299	46	1538	46	1884	68	69

https://doi.org/10.1017/S0263593300001176 Published online by Cambridge University Press

Table 4a–d *Continued*

	Analysis no.	Zircon type	U (ppm)	Th (ppm)	Th/U	Pb* (ppm)	204 / ppb	$^{204}Pb/^{206}Pb$	f_{206} %	Radiogenic rates $^{206}Pb/^{238}U$	±	$^{207}Pb/^{235}U$	±	$^{207}Pb/^{206}Pb$	±	Ages (in Ma) $^{206}Pb/^{238}U$	±	$^{207}Pb/^{235}U$	±	$^{207}Pb/^{206}Pb$	±	Conc.%
Gr3	3·2	C2	67	110	1·63	34	2	0·000106	0·147	0·528	0·011	11·69	0·32	0·1605	0·0025	2735	47	2580	26	2461	27	111
	5·1	C2	73	34	0·47	21	1	0·000084	0·116	0·3841	0·0076	7·96	0·43	0·1504	0·0072	2095	35	2227	50	2350	84	89
	6·1	C1	47	96	2·06	26	5	0·000321	0·445	0·537	0·015	11·56	0·55	0·1561	0·0056	2773	62	2570	46	2413	62	115
	7·2	C1	43	4	0·08	25	0	—	<0·01	0·714	0·015	15·76	0·45	0·1600	0·0027	3474	58	2862	28	2456	29	142
	8·1	C2	61	26	0·42	24	0	0·000010	0·014	0·520	0·014	11·28	0·58	0·1574	0·0064	2697	58	2546	49	2428	71	111
	15·1	R1	36	12	0·32	15	4	0·000327	0·453	0·591	0·024	11·87	0·97	0·1456	0·0097	2994	97	2594	80	2295	119	131
	23·2	R1	77	7	0·09	39	3	0·000100	0·136	0·616	0·015	13·18	0·40	0·1552	0·0023	3094	61	2693	29	2404	26	129
	25·1	R1	109	29	0·27	37	4	0·000118	0·16	0·406	0·011	8·08	0·32	0·1442	0·0039	2199	49	2240	37	2278	48	97
	30·1	R1	15	2	0·15	6	0	0·000073	0·099	0·499	0·025	10·90	0·75	0·1583	0·0066	2611	108	2515	66	2438	72	107
Gr4	4·2	R1	39	39	1·02	5	0	0·000023	0·039	0·1612	0·0039	1·67	0·06	0·0752	0·0019	963	22	997	24	1073	50	90
	4·3	R1	28	8	0·30	3	1	0·000283	0·485	0·1513	0·0051	1·78	0·12	0·0855	0·0048	908	28	1039	46	1327	112	68
	4·4	R1	28	19	0·68	3	0	0·000151	0·258	0·1539	0·0064	1·63	0·11	0·0767	0·0035	923	36	981	42	1113	93	83
	12·1	R1	29	13	0·43	3	4	0·001637	2·806	0·1543	0·0058	1·44	0·28	0·068	0·013	925	33	906	124	859	443	108
	13·1	R1	42	19	0·46	4	4	0·001006	1·724	0·1525	0·0051	1·21	0·15	0·0578	0·0067	915	28	807	72	521	276	176
	13·2	R1	51	23	0·45	6	1	0·000255	0·437	0·1521	0·0036	1·49	0·06	0·0709	0·0023	913	20	925	27	955	69	96
	20·1	R1	28	13	0·48	4	1	0·000417	0·697	0·1526	0·0058	1·67	0·14	0·0793	0·0054	916	32	997	53	1179	140	78
	23·1	R1	61	24	0·40	7	3	0·000488	0·816	0·1494	0·0036	1·41	0·06	0·0682	0·0024	898	20	891	27	875	74	103
	26·1	R1	42	13	0·31	5	3	0·000561	0·939	0·1584	0·0044	1·50	0·07	0·0685	0·0026	948	25	929	31	885	80	107
(c) Sample OG473																						
Gr1	1·2	C1	509	98	0·19	311	2	0·000011	0·013	0·773	0·010	31·44	0·43	0·2951	0·0007	3691	37	3533	14	3445	4	107
	7·1	C1	375	273	0·73	183	4	0·000031	0·042	0·5924	0·0082	16·57	0·31	0·2029	0·0023	2999	33	2910	18	2849	18	105
	8·1	C1	759	247	0·33	428	4	0·000012	0·015	0·693	0·011	28·47	0·61	0·2978	0·0037	3395	43	3435	21	3459	19	98
Gr2	1·1	R1	79	147	1·87	49	2	0·000074	0·099	0·628	0·012	17·45	0·40	0·2016	0·0018	3142	49	2960	22	2839	15	111
	2·2	R1	81	71	0·87	27	2	0·000114	0·155	0·357	0·011	7·00	0·32	0·1421	0·0045	1970	51	2112	41	2253	55	87
	7·2	R1	88	68	0·77	45	3	0·000078	0·109	0·635	0·012	14·32	0·48	0·1636	0·0042	3170	46	2771	32	2493	44	127
	9·1	C1	270	185	0·69	122	4	0·000046	0·063	0·5634	0·0076	14·51	0·23	0·1867	0·0012	2881	32	2783	15	2713	11	106
	11·1	C1	334	436	1·31	163	0	—	<0·01	0·5421	0·0087	12·10	0·21	0·1619	0·0009	2792	37	2612	17	2476	9	113
	13·1	R1	79	50	0·63	29	0	0·000010	0·014	0·455	0·012	11·48	0·44	0·1829	0·0044	2419	55	2563	36	2679	41	90
	13·2	C3	159	120	0·76	55	2	0·000060	0·081	0·4174	0·0064	9·62	0·38	0·1671	0·0058	2249	29	2399	37	2529	59	89
	14·1	C2	560	837	1·49	269	0	—	<0·01	0·5147	0·0065	12·04	0·19	0·1696	0·0012	2676	28	2607	15	2554	12	105
	15·1	R1	86	112	1·31	23	2	0·000137	0·182	0·288	0·010	7·44	0·39	0·1871	0·0066	1633	52	2165	49	2717	59	60
	15·2	R2	158	107	0·68	51	1	0·000021	0·029	0·3805	0·0075	7·94	0·19	0·1513	0·0018	2079	35	2224	22	2361	21	88
	15·3	C2	137	228	1·66	75	0	—	<0·01	0·4917	0·0097	11·66	0·29	0·1720	0·0023	2578	42	2577	24	2577	23	100
	16·1	C2	184	181	0·98	76	3	0·000049	0·069	0·499	0·012	10·66	0·36	0·1550	0·0032	2608	52	2494	32	2402	35	109
	17·1	R2	197	127	0·64	55	2	0·000056	0·073	0·3539	0·0060	10·50	0·22	0·2151	0·0023	1953	28	2480	20	2945	17	66
	18·1	R2	189	122	0·64	39	2	0·000066	0·09	0·2271	0·0056	3·72	0·13	0·1188	0·0027	1319	30	1575	29	1938	41	68
	19·1	R1	92	77	0·83	47	1	0·000028	0·038	0·517	0·013	12·46	0·48	0·1749	0·0046	2686	56	2640	37	2605	44	103
	20·1	R1	72	43	0·60	17	1	0·000046	0·07	0·2596	0·0066	4·26	0·14	0·1189	0·0022	1488	34	1685	28	1940	34	77
	21·1	R1	144	137	0·95	123	2	0·000024	0·033	0·882	0·019	20·57	0·74	0·1691	0·0044	4077	67	3118	36	2549	44	160
	22·1	R1	92	72	0·78	21	2	0·000135	0·212	0·2533	0·0042	3·73	0·14	0·1067	0·0034	1456	21	1577	31	1745	60	83
	23·1	R1	131	88	0·67	28	2	0·000104	0·164	0·2376	0·0043	3·718	0·082	0·1135	0·0012	1374	22	1575	18	1856	19	74
	23·2	R1	88	78	0·89	60	3	0·000066	0·09	0·716	0·013	17·09	0·36	0·1730	0·0013	3482	51	2940	20	2587	12	135
	24·1	C2	121	102	0·84	61	2	0·000038	0·052	0·5288	0·0088	13·12	0·32	0·1800	0·0028	2736	37	2688	23	2652	26	103
	25·1	R1	95	85	0·89	24	4	0·000222	0·301	0·2712	0·0042	5·65	0·18	0·1511	0·0038	1547	21	1924	27	2358	44	66
	27·1	R1	99	82	0·82	45	1	0·000044	0·06	0·4736	0·0086	10·84	0·22	0·1660	0·0012	2499	38	2509	19	2518	12	99
	28·1	R1	110	52	0·47	47	0	—	<0·01	0·4894	0·0072	10·80	0·18	0·1600	0·0012	2568	31	2506	16	2456	12	105
	10·1	C3	341	235	0·69	127	1	0·000008	0·011	0·4560	0·0063	12·26	0·31	0·1950	0·0038	2422	28	2624	24	2785	33	87
	26·1	C2	153	323	2·10	180	1	0·000010	0·014	0·9942	0·0309	26·25	1·36	0·1915	0·0072	4450	101	3356	52	2755	64	162
Gr3	6·1	R2	548	484	0·88	125	0	0·000004	0·007	0·2869	0·0036	3·910	0·055	0·0989	0·0005	1626	18	1616	11	1603	9	101
	12·1	R1	98	64	0·65	22	5	0·000275	0·437	0·2915	0·0049	4·028	0·098	0·1002	0·0016	1649	24	1640	20	1628	30	101
	12·2	R1	104	66	0·64	26	3	0·000135	0·212	0·2831	0·0050	3·817	0·088	0·0978	0·0012	1607	25	1596	19	1582	24	102
	2·1	R2	262	145	0·55	31	1	0·000037	0·063	0·1616	0·0022	1·679	0·037	0·0754	0·0012	966	12	1001	14	1078	31	90
Gr4	3·1	R2	2090	135	0·06	212	8	0·000041	0·069	0·1589	0·0018	1·556	0·020	0·0710	0·0004	951	10	953	8	958	11	99
	4·1	R2	3532	147	0·04	369	0	—	<0·01	0·1646	0·0017	1·587	0·020	0·0699	0·0004	982	10	965	8	926	11	106
	4·2	R2	2796	175	0·06	278	3	0·000012	0·021	0·1560	0·0017	1·502	0·019	0·0698	0·0004	935	9	931	8	923	12	101
	4·3	R2	2482	154	0·06	250	4	0·000018	0·031	0·1582	0·0018	1·524	0·019	0·0699	0·0003	947	10	940	8	925	9	102
	5·1	R2	3126	193	0·06	306	2	0·000006	0·01	0·1536	0·0016	1·483	0·018	0·0700	0·0003	921	9	923	7	929	9	99
	5·2	R2	4919	205	0·04	483	3	0·000006	0·011	0·1547	0·0017	1·484	0·018	0·0696	0·0003	927	9	924	8	915	10	101
	5·3	R2	2412	145	0·06	215	8	0·000041	0·071	0·1393	0·0015	1·350	0·018	0·0703	0·0004	841	9	867	8	936	12	90

https://doi.org/10.1017/S0263593300001176 Published online by Cambridge University Press

Table 4a–d *Continued*

	Analysis no.	Zircon type	U (ppm)	Th (ppm)	Th/U	Pb* (ppm)	204 / ppb	$^{204}Pb/^{206}Pb$	f_{206} %	Radiogenic rates $^{206}Pb/^{238}U$	±	$^{207}Pb/^{235}U$	±	$^{207}Pb/^{206}Pb$	±	Ages (in Ma) $^{206}Pb/^{238}U$	±	$^{207}Pb/^{235}U$	±	$^{207}Pb/^{206}Pb$	±	Conc.%
(d) Sample OG471																						
Gr1	1·1	C1	445	382	0·86	167	1	0·000011	0·015	0·4593	0·0054	9·81	0·13	0·1550	0·0007	2436	24	2417	12	2401	8	102
	2·1	C1	265	104	0·39	82	0	0·000007	0·01	0·4234	0·0058	8·19	0·12	0·1402	0·0007	2276	26	2252	14	2230	9	102
	3·2	C1	192	156	0·81	68	3	0·000071	0·102	0·4360	0·0059	8·89	0·13	0·1478	0·0008	2333	27	2326	14	2321	9	101
	4·2	C1	289	128	0·44	78	3	0·000045	0·068	0·3665	0·0044	6·313	0·087	0·1249	0·0007	2013	21	2020	12	2028	10	99
	8·1	C2	347	28	0·08	99	0	—	<0·01	0·4196	0·0054	8·03	0·12	0·1388	0·0007	2259	25	2235	13	2213	9	102
	12·1	R1	147	158	1·07	63	1	0·000024	0·033	0·4901	0·0082	11·56	0·32	0·1711	0·0034	2571	36	2570	26	2568	33	100
	13·1	C2	230	466	2·03	111	2	0·000038	0·054	0·4774	0·0059	10·65	0·14	0·1617	0·0007	2516	26	2493	13	2474	7	102
	15·1	C2	227	408	1·79	76	3	0·000062	0·088	0·3454	0·0050	6·65	0·12	0·1397	0·0012	1913	24	2066	16	2223	15	86
	17·1	R1	168	128	0·76	52	1	0·000030	0·043	0·3852	0·0054	7·98	0·14	0·1503	0·0013	2101	25	2229	16	2350	15	89
	18·1	R1	114	67	0·59	51	1	0·000016	0·022	0·579	0·010	12·69	0·25	0·1588	0·0011	2946	41	2657	18	2443	11	121
Gr2	2·2	R1	142	129	0·91	34	0	—	<0·01	0·2968	0·0044	4·110	0·078	0·1004	0·0010	1676	22	1656	16	1632	19	103
	3·1	R1	149	144	0·96	42	2	0·000080	0·127	0·3488	0·0052	4·905	0·088	0·1020	0·0009	1929	25	1803	15	1661	16	116
	4·1	R1	157	143	0·91	27	2	0·000118	0·186	0·2151	0·0042	2·630	0·069	0·0887	0·0014	1256	22	1309	19	1397	30	90
	9·1	R1	293	133	0·45	55	3	0·000068	0·108	0·2670	0·0032	3·426	0·054	0·0930	0·0008	1526	16	1510	12	1489	16	103
	14·1	R1	233	149	0·64	52	1	0·000029	0·045	0·2964	0·0039	3·873	0·069	0·0948	0·0010	1673	19	1608	14	1524	20	110
	20·1	R1	341	174	0·51	66	1	0·000019	0·031	0·2630	0·0034	3·631	0·057	0·1001	0·0007	1505	17	1556	13	1627	14	93
Gr3	1·2	R1	204	174	0·85	24	2	0·000109	0·188	0·1496	0·0021	1·376	0·028	0·0667	0·0009	899	11	879	12	829	29	108
	5·1	R1	239	26	0·11	22	2	0·000111	0·193	0·1400	0·0020	1·290	0·025	0·0668	0·0008	845	12	841	11	832	24	102
	6·1	R1	173	146	0·85	21	1	0·000095	0·164	0·1533	0·0020	1·504	0·028	0·0711	0·0008	920	11	932	11	961	24	96
	7·1	R1	213	177	0·83	25	2	0·000104	0·179	0·1512	0·0022	1·417	0·030	0·0680	0·0009	908	13	896	12	868	27	105
	10·1	R1	234	194	0·83	25	1	0·000056	0·098	0·1400	0·0020	1·273	0·028	0·0659	0·0010	845	11	834	13	804	33	105
	11·1	R1	445	330	0·74	34	1	0·000045	0·079	0·1006	0·0012	0·864	0·015	0·0623	0·0007	618	7	632	8	684	24	90
	16·1	R1	175	143	0·82	20	2	0·000103	0·178	0·1505	0·0025	1·407	0·052	0·0678	0·0021	904	14	892	22	863	67	105
	19·1	R1	217	194	0·89	25	0	0·000014	0·024	0·1437	0·0026	1·354	0·033	0·0683	0·0010	866	15	869	14	878	30	99

Notes: (1) Uncertainties given at the 1 σ level; (2) f_{206} % denotes the percentage of ^{206}Pb that is common Pb; (3) Correction for common Pb made using the measured $^{204}Pb/^{206}Pb$ ratio; (4) For % Conc., 100% denotes a concordant analysis. >100% indicates reverse discordance; (5) 'Group' (Gr) refers to a particular age population and may include one or more zircon texural type.

5. Discussion

5.1. Interpretation of zircon ages

Based on the distribution of data and ages in the samples discussed here, it is difficult to establish a solid event chronology or accurately constrain the ages of fabrics or events in the Oygarden Group, prior to the ~930 Ma RSE. These problems are exacerbated by a general lack of oscillatory zoned zircon grains in orthogneiss samples such that intrusive ages could not be established, and also by the intensity of recrystallisation, both tectonically and of zircon grains that affected the area during the RSE. However, some information regarding the early history of the Oygarden Group can be gleaned from the data (Table 5).

The predominance of zircon cores in OG615 (C3) have internal textures that are interpreted to reflect growth from or in the presence of melt, suggesting that these zircon grains may have grown during the development of leucocratic segregations preserved in this rock either prior to or during the development of S_1. The maximum age of these grains (~3650 Ma) provides a minimum age for the igneous protolith to OG615, and the approximate age of this melting event. Inherited magmatic grains in OG525 and OG473 indicate that an event at this time was accompanied, and/or followed by magmatism. However, the relatively small fraction of the early Archaean zircon grains inherited by OG525 and OG473 orthogneiss, when compared to non-inherited zircon, suggests that the early (≥3650 Ma) Archaean-aged orthogneiss within the *LCO* may not a constitute major proportion of the exposed crust in the Oygarden region. The distribution of data in OG615 also indicates that a second thermal event affected the Oygarden area at ~3470 Ma. Although it is difficult to assign this age to a particular event, this age may reflect the development of S_1 and alignment of leucocratic segregations. *HFO* (OG525) cuts S_1, but contains an intense S_2 foliation, suggesting emplacement after D_1, and either before or during a D_2 event. In common with all orthogneiss samples studied here, few magmatic zircon grains were recovered from this sample. This suggests that the metamorphic event that occurred at ~2780 Ma was intense enough to recrystallise nearly all magmatic zircon originally present. As such, the crystallisation age of the protolith to this orthogneiss remains obscure. However, it most likely occurred at some time after ~3470 Ma and before the maximum age of 'metamorphic' zircon in the rock (~2780 Ma). The distribution of data from OG473, which preserves possible evidence for metamorphic zircon up to ~2840 Ma, suggests that components of the *HFO* may have protoliths older than this age.

These data are indicative of an extended evolution for both the *LCO* and *HFO* lithologies. OG615 represents only one layer of the *LCO*, and where intruded by OG525 provides a rare example of a cross-cutting relationship between *LCO* and *HFO*. Moreover, sample OG473, which was taken from a homogeneous felsic orthogneiss layer within the *LCO*, has inherited magmatic zircon grains ~3500 Ma in age, suggesting this orthogneiss is younger than some components of the *LCO* (e.g., OG615, which has metamorphic zircon >3600 Ma). Therefore, the *LCO* comprises components that are both older (OG615) and younger (OG473) than D_1. Tectonic transposition and recrystallisation of layers during D_2 and D_3 events has destroyed most internal relationships making further discrimination unfeasible.

Due to a lack of textural context for these zircon grains, it is difficult to link the age of 'metamorphic' zircon in the HFO to

https://doi.org/10.1017/S0263593300001176 Published online by Cambridge University Press

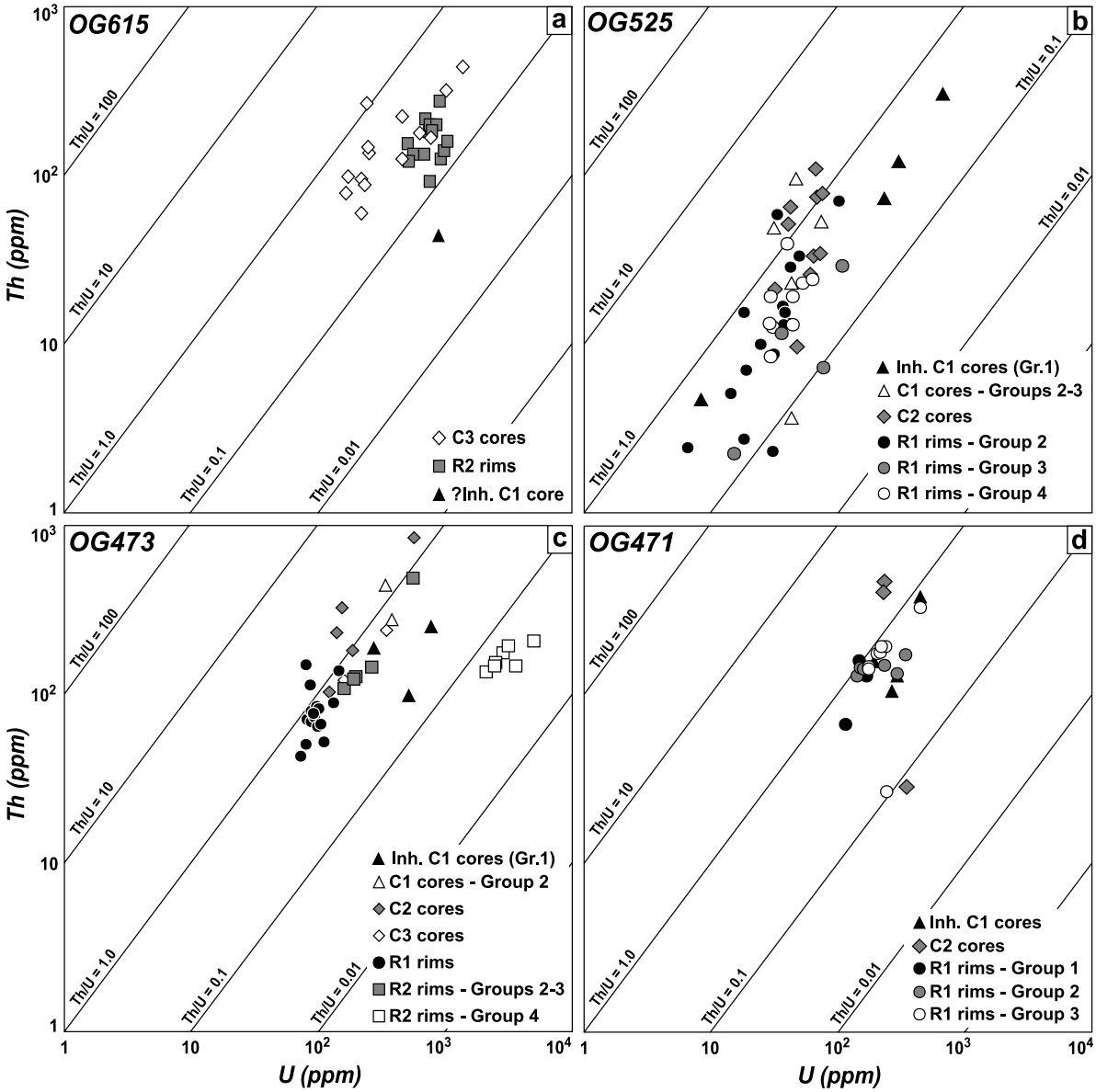

Figure 5 Th vs U diagrams for each sample, depicting the chemical distribution between zircon types defined in the text and Table 1.

the development of S_2. However, we can 'see' evidence for metamorphic growth or modification of pre-existing zircon grains during multiple events culminating in the well-constrained RSE at ~930–910 Ma (Kelly *et al.* 2002). In OG525, the upper intercept of a regression through discordant data from C2 cores and R1 rims (~2780 Ma) provides a minimum but probable age of the C2 cores, and the possible timing age of the S_2 gneissosity. However, the timing of R1 rim formation is more problematic. In OG525, although data from R1 rims form part of the major discordia that between ~2780 and ~930 Ma, discordant ages from R1 rims also occur between ~2400 and ~930 Ma. A simple explanation may be that these rims developed during the intense reworking of crust during the RSE. However, a concordant age from an R1 rim near the upper intercept (~2733 Ma) and the presence of inherited Palaeoproterozoic-aged R1 rims in the pegmatite sample (OG471), suggest that while intense isotopic resetting of zircon may have occurred at ~930 Ma, the development of these rims occurred earlier, possibly at ~2780 Ma. The presence of R1 rims at ~2400–2500 Ma, ~1600 Ma and ~930 Ma in multiple samples indicates that these rims could possibly have formed at multiple times during the evolution of the terrane and the processes that led to their formation are not unique to a single event. Alternatively, it is possible that the development of these rims, for example at ~2780 Ma, made them highly susceptible to resetting during subsequent thermal events.

Subsequent thermal events can be seen recorded in the data during the Palaeo- and Mesoproterozoic. Small clusters of concordant data in OG615, discordant data from C2 cores and R1 rims in OG525, and scattered data from similar zircon types in OG473 are suggestive of either growth and/or isotopic disturbance of zircon grains at ~2400–2300 Ma. Whilst these data are too scattered and imprecise to pin to a particular event, they do indicate a thermal event at this time in the Oygarden Group. More convincing are concordant data from R2 rims in OG615, R1 rims in OG473 and scattered and discordant inherited ages from 'metamorphic' zircon in OG471, which suggest an event at ~1600 Ma. These ages correlate with inherited magmatic zircon in a syn-D_4 pegmatite from the Oygarden Group (Kelly *et al.* 2002) and indicate that an event involving

https://doi.org/10.1017/S0263593300001176 Published online by Cambridge University Press

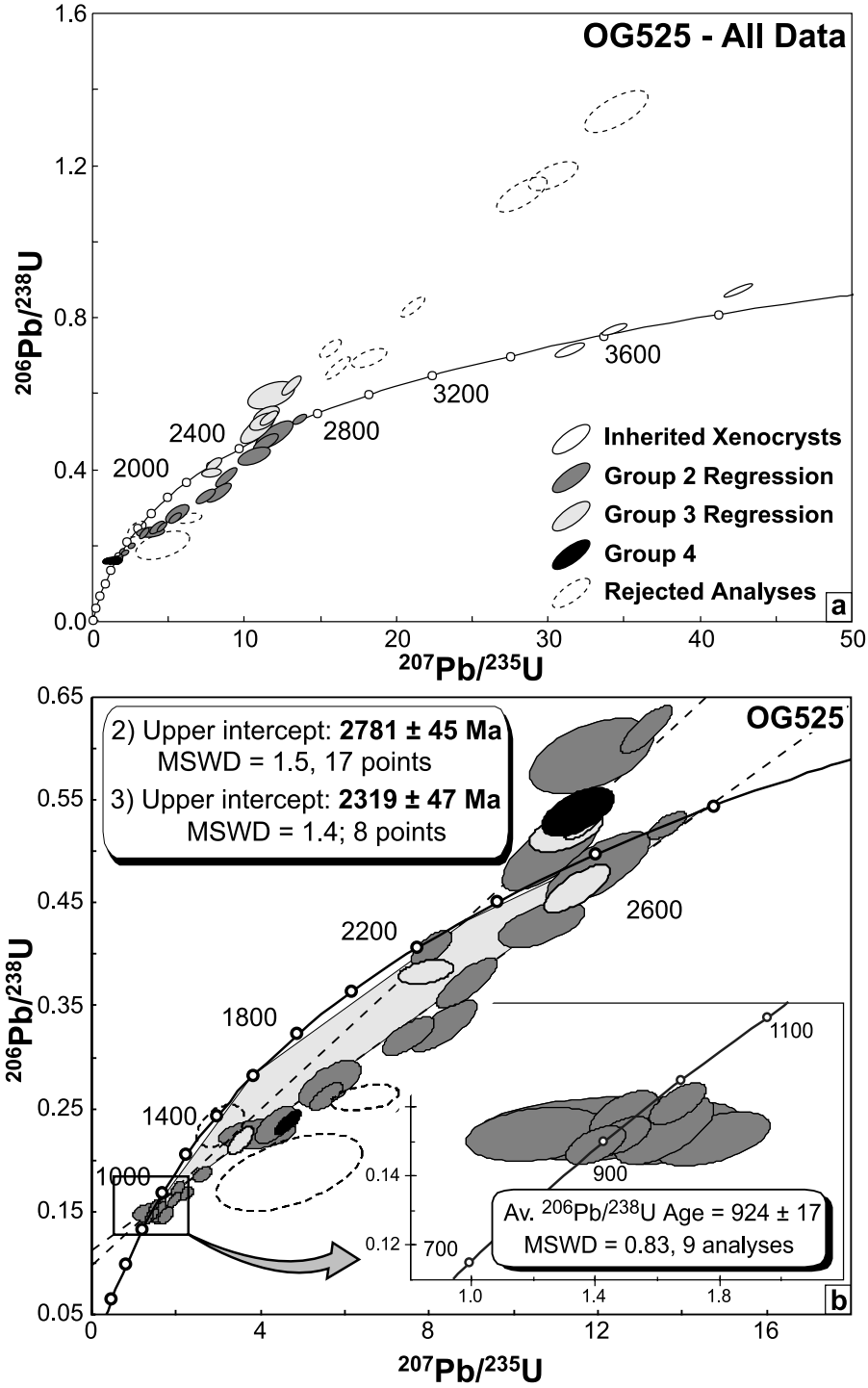

Figure 6 (a) Standard Wetherill concordia diagram showing the distribution of U–Pb data from sample OG525. One failed analysis (1·1; Table 4b) of an inherited core is not plotted. Error ellipses are shaded according to Group, except those rejected from age analysis, which are indicated by unfilled ellipses with dashed outlines. (b) Enlarged view of (a). U–Pb data show two lines of mixing that project from Late Archaean and Palaeoproterozoic ages towards ~930 Ma. Regression 1 is through ages with an upper intercept of ~2780 Ma, and regression 2 is through data with an upper intercept of ~2320 Ma. Data rejected from both regressions are indicated by unfilled ellipses with dashed outlines. Shaded symbols: (black) C1 cores; (dark grey) R1 rims; (light grey) C2 cores. *Inset*: cluster of data at ~924 Ma (from Kelly *et al.* 2002).

both metamorphism and magmatism affected the area at this time.

What is clear from the data presented here, is that evidence exists for multiple thermal events that are not recognisable as foliations or structures in the field. Whilst evidence for S_1 exists in rare low strain windows, S_2 is mostly manifested as a layer-parallel gneissosity that reflects the complete transposition of all earlier structures. What is now observed as S_2 either represents the culmination of multiple deformation events, or complete transposition during an event prior to the RSE at ~930 Ma.

5.2. Archaean crust in the Rayner Complex

Zircon ages from orthogneiss in the Oygarden Group indicate the predominance of Archaean crust in an area that was tectonically reworked during the early Neoproterozoic RSE. These ages broadly correlate with areas immediately adjacent to the Oygarden Islands, and add to the currently evolving

https://doi.org/10.1017/S0263593300001176 Published online by Cambridge University Press

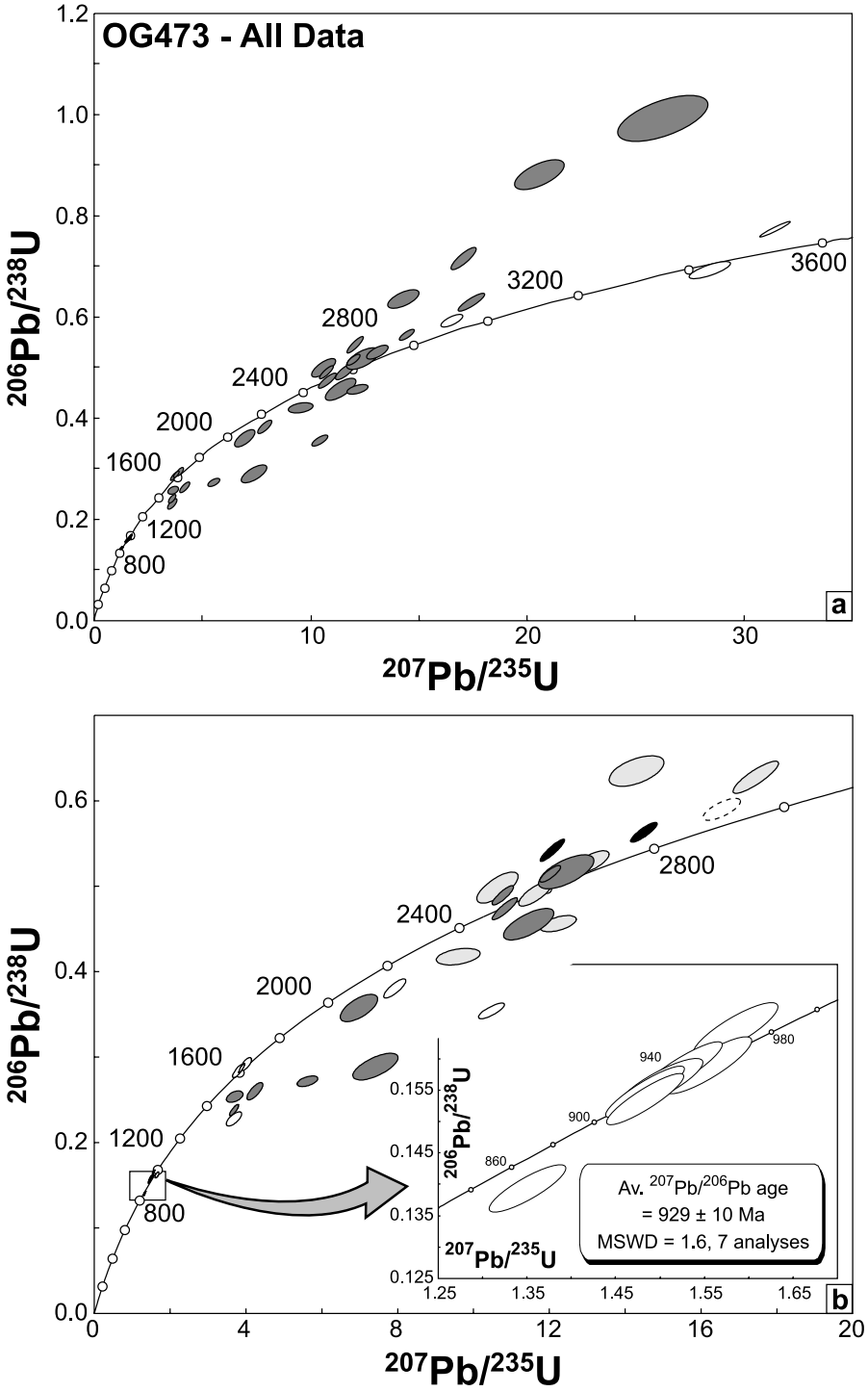

Figure 7 (a) Standard Wetherill concordia diagram showing the distribution of all U–Pb data from sample OG473. Shaded symbols: (white) inherited cores; (dark grey) remaining data. (b) Enlarged view of (a): U–Pb data show no clear lines of mixing in the large scatter between Late Archaean and younger, Proterozoic ages. Shaded symbols: (dashed) inherited; (black) C1 cores; (dark grey) R1 rims; (light grey) C2/C3 cores; (white) R2 rims. *Inset*: cluster of data from R2 rims at ~930 Ma (from Kelly *et al.* 2002).

framework for a regional geological evolution. Components of the *LCO* in the Oygarden Group have a protolith age older than ~3650 Ma. It is possible that the protolith to the *LCO* is comparable in age to ~3800 Ma orthogneiss in the Napier Complex (Black *et al.* 1986; Harley & Black 1997), although this is purely speculative. The ~3650 Ma metamorphic age from this sample is an age that is comparatively rare in East Antarctica. However, more Early to Middle Archaean ages are beginning to emerge from the Napier Complex, including ~3650 Ma detrital ages from metasediments (Mt Cronus; Asami *et al.* 2002) and ~3300 Ma ages from tonalites (Mt Riiser Larsen; Hokada *et al.* 2003). The protolith to *HFO* (OG525) was emplaced in the Oygarden Group at some time before ~2780, and was metamorphosed at high-grade conditions at this time. This age as yet does not correlate with early metamorphism or magmatism in the Napier Complex. However, there is some indication for zircon grains with ages up to ~2840 Ma, a time of regional metamorphism and magmatism in the Napier Complex (Harley & Black 1997). These Late Archaean ages are also broadly similar to the age of the Stillwell Hills orthogneiss (~2700 Ma, Rb-Sr whole rock age; Clarke 1987). This unit is nearly identical in appearance to

https://doi.org/10.1017/S0263593300001176 Published online by Cambridge University Press

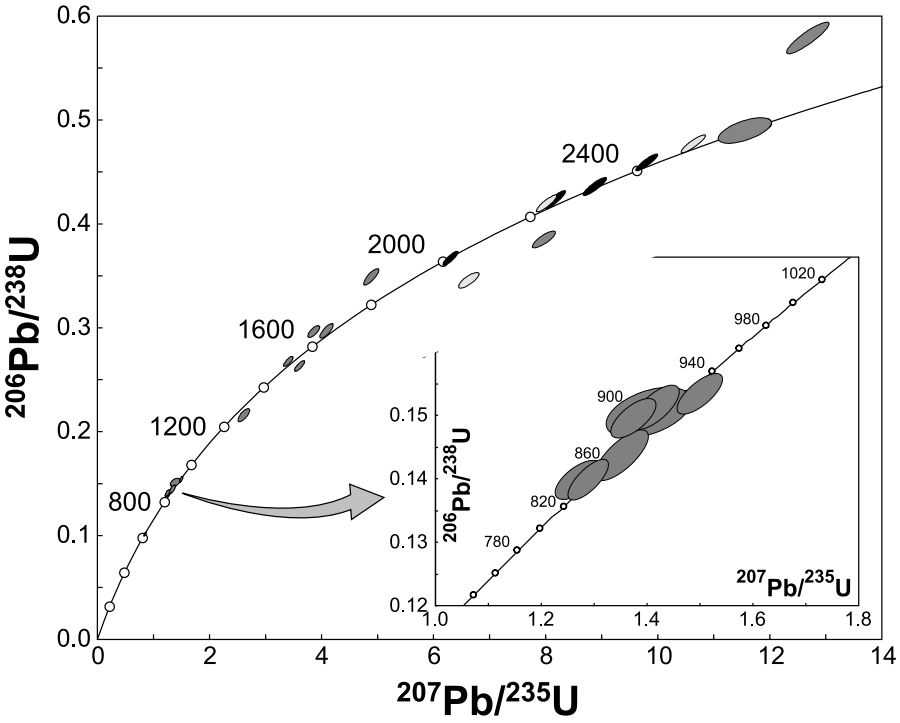

Figure 8 Standard Wetherill concordia diagram showing the distribution all U–Pb data from sample OG471. The data show a smear of ages between ~2600 Ma and ~1400 Ma. Shaded symbols: (black) C1 cores; (dark grey) R1 rims; (light grey) C2 cores. *Inset*: cluster of data at ~900 Ma (from Kelly *et al.* 2002).

Table 5 Summary of U-Pb SHRIMP ages and event history

Age	Interpretation	Event 1 scenario	Event 2 scenario	Correlation with Napier Complex
?3650	protolith to felsic orthogneiss within layered composite orthogneiss (OG615)			?3800 Ma?
~3650 Ma	metamorphism and anatexis (OG615); accompanied by magmatism (inherited grains in OG525/OG473)	D_1/S_1	*Early Met-1*	
3650–3470 Ma	partial resetting of isotopic ratios in zircons (OG615)		*Early Met-2*	
>2840–2780 Ma	protolith to homogeneous felsic orthogneiss (OG525/OG473)	?pre- or syn-D_2 intrusion?	?pre- or syn-D_1 intrusion?	*c.* 2840 Ma
~2780 Ma	metamorphism (OG525/OG473)	D_{2a}/S_2	D_1/S_1	<2840 Ma
~2400 Ma	metamorphism (OG615/OG525/OG473)	D_{2b}	D_{2a}/S_2	?2570–2480 Ma?
~1600 Ma	metamorphism & magmatism (OG525/OG473/OG435*)	D_{2c}	D_{2b}	
930–910 Ma	deformation, metamorphism & anatexis associated with the RSE (OG525/OG473/OG471*/OG435*/OG636*)	D_{3-D4}	D_{3-D4}	

*denotes sample described in Kelly *et al.* (2002).

parts of *LCO* in the Oygarden Islands (N. M. Kelly, unpublished field observations) and was correlated with this unit by Trail (1970).

More abundant evidence exists for a regional metamorphic and magmatic event between ~2500 Ma and ~2400 Ma. Rb/Sr whole rock ages of ~2500 Ma were derived from depleted granite and garnet gneiss from Edward VIII Gulf, and were interpreted to represent high-grade metamorphism that affected ~3100 Ma tonalitic gneisses in that area (Sheraton & Black 1983). This age also represents a period of widespread metamorphism and magmatism in the Napier Complex between 2550 and 2400 Ma (Black & James 1982; Grew *et al.* 1982; Black *et al.* 1986; Sheraton *et al.* 1987; Harley & Black 1997; Asami *et al.* 2002; Carson *et al.* 2002c). Although data from Oygarden Group orthogneiss samples are imprecise, data distribution and Pb-loss patterns do reflect the effects of a thermal event that affected the Oygarden Group at this time.

The age estimates from the Oygarden Group contrast markedly with crustal ages from the Rayner Complex in western Enderby Land, Mawson Coast and northern Prince Charles Mountains (Fig. 1). Orthogneiss rocks in these areas are dominated by Paleoproterozoic Nd model ages and do not preserve evidence for Archaean material (Black *et al.* 1987; Young & Black 1991; Young *et al.* 1997). The similarity of protolith and metamorphic ages for rocks on coastal outcrops between Edward VIII Gulf and the Stillwell Hills, and disparity with the Mawson Coast and northern Prince Charles Mountains, suggests that Kemp Land forms part of a separate terrane with an Archaean history. Archaean ages for felsic orthogneiss in the Stillwell Hills and the lack of Archaean protolith ages to the east of that location (e.g. Cape Bruce,

https://doi.org/10.1017/S0263593300001176 Published online by Cambridge University Press

Mawson, northern Prince Charles Mountains) supports the interpretation that a terrane boundary lies between predominantly Archaean crust in Kemp Land and Mesoproterozoic crust in MacRobertson Land, as originally proposed by Dunkley (1998). This boundary most likely lies in the vicinity of the Stillwell Hills.

5.3. Interpretation of Th/U ratios in 'metamorphic' zircon

When assigning the meaning of an age obtained from 'metamorphic' zircon, it becomes important to understand how such zircon may have formed. It has been common to use chemical indicators such as Th/U ratios to suggest that particular zircon grains grew during metamorphism (e.g. Rubatto & Gebauer 2000; Hermann *et al*. 2001). Zircon grains from the Oygarden samples preserve evidence for a number of different morphologies and textural types that are interpreted to have formed through different processes associated with metamorphism. For example, sector zoned and planar banded (C3) zircon cores are similar to grains described by other authors (e.g. Vavra *et al*. 1996, 1999; Kelly *et al*. 2002) and are commonly interpreted to reflect growth from or in the presence of anatectic melt during high-grade metamorphism. The range of Th/U ratios observed for these grains (0·21–1·09) may be explained by fluctuating elemental abundance in an anatectic melt. In contrast to these grains, the ovoid and anhedral morphology of C2 zircon cores, and their relatively homogeneous internal texture, is typical of zircon that has grown through sub-solidus metamorphic processes (Watson & Liang 1995; Vavra *et al*. 1996; Schaltegger *et al*. 1999). However, the Th/U composition of these grains (0·2–1·63) is not indicative of the low (<0·1) and tightly clustered values suggested by some authors for 'metamorphic' zircon (e.g. Rubatto & Gebauer 2000). We suggest that this spread in ratios reflects recrystallisation of pre-existing zircon and not new growth. This interpretation is supported by the general lack of magmatic zircons preserved in the two *HFO* samples studied. The range of Th/U ratios may then reflect a vestige of the original Th/U of the primary grain later influenced by recrystallisation or annealing, a process not yet fully understood (Pidgeon *et al*. 1998; Schaltegger *et al*. 1999; Hoskin & Black 2000).

The development of R1 rims, which are ubiquitous to the orthogneiss samples OG525 and OG473, but also present in OG471, is also problematic. These rims, which are typically highly luminescent, embay along curved fronts and may preserve 'ghost zoning'. Importantly, R1 rims commonly have a broad range of Th/U ratios within and between samples (0·07–1·87) and can be much higher than typically inferred for metamorphic zircon. The U concentrations of R1 rims are typically lower than the cores they occur on, although Th concentrations vary non-systematically. These features are not consistent with sub-solidus metamorphic growth but reflect partial to complete recrystallisation and/or annealing of the margins of zircon grains during metamorphism. The bleached R1 rims described here are texturally similar to features described by Harley *et al*. (1998), Schaltegger *et al*. (1999),Vavra *et al*. (1999) and Crowe *et al*. (2002), and where they were inferred to reflect recrystallisation through progressive replacement of previous structures by secondary domains defined by curved phase boundaries. Localised ingress and leaching by a chemically aggressive fluid is interpreted to be the cause of replacement, which may enhance the mobility of U, Th and Pb in undamaged zircon (Schaltegger *et al*. 1999; Vavra *et al*. 1999). Alternatively, these rims may have formed through solid-state recrystallisation without sub-grain rotation or dissolution and re-precipitation, and therefore not via a fluid-dominated mechanism (Hoskin & Black 2000).

Type R2 rims, which also commonly preserve a homogeneous internal texture typical of metamorpic growth, may be further subdivided in OG473. In this sample, R2 rims fall into low Th/U (0·04–0·06) and high Th/U types (0·64–0·88). The latter grouping are all >1000 Ma in age and are commonly discordant. The former cluster at ~930 Ma and are nearly all concordant. Th and U are interpreted to be 'incompatible' elements with respect to zircon, and are more likely to be lost than to diffuse into a zircon during metamorphic recrystallisation (Schaltegger *et al*. 1999). The homogeneous textural and chemical nature of metamorphic rims is commonly interpreted to reflect sub-solidus growth where the local equilibration volume is likely to have been more chemically uniform compared to the fluctuating levels that may occur in a melt over time. The distinct Th-U composition, in particular the high U concentration of some R2 rims, suggests they are probably the result of *new* growth and not recrystallisation of pre-existing zircon. In comparison, R2 rims with higher, more scattered Th/U ratios may reflect formation through recrystallisation. The low, uniform Th/U values preferred by some authors to characterise 'metamorphic' zircon, may then be applicable only to *new* zircon that formed through *sub-solidus* growth. However, the resulting signature will still be dependent on the local chemical and metamorphic reaction environment. Th/U ratios may therefore be important indicators in the interpretation of the origin of different 'metamorphic' zircon types.

6. Conclusions

Multiple high-grade events affected the Oygarden area in the Early to Late Archaean and the Proterozoic, creating complex arrays of U-Pb data. Careful interpretation of data has provided some insight into the early history of the Oygarden Group. The oldest lithology in the area is the *LCO*, part of which is older than ~3650 Ma. This age is represented by the crystallisation of zircon from an anatectic melt during metamorphism and is interpreted to reflect the development of S_1 leucosome. *LCO* was also affected by a thermal event at ~3470 Ma, causing isotopic disturbance in ~3650 Ma zircon grains. The *HFO* intruded following D_1 and but before ~2780 Ma, and was affected by metamorphism at ~2780 Ma. Subsequent thermal events, including those at ~2400 and ~1600 Ma, caused the partial resetting of isotopic ratios in OG473 and OG525. However isotopic disturbance of zircon grains during the RSE at ~930 Ma is interpreted to be the dominant Pb-loss event.

7. Acknowledgments

The authors wish to acknowledge careful reviews by T. Hokada and M. Whitehouse for improving the quality and content of this paper, and K. Mezger, P. Dirks and I. Fitzsimons who provided helpful comments on earlier versions of the manuscript. This work was completed with funding from the Antarctic Science Advisory Committee (GLC & S.L. Harley; ASAC Project No's. 2214 & 1150). Fieldwork was conducted during the 1996/7 and 1997/8 Australian National Antarctic Research Expeditions. The Australian Antarctic Division and the personnel of Mawson Base are thanked for logistic support. NMK gratefully acknowledges the support of a University of Sydney Postgraduate Research Award (1996–2000) and a Royal Society of Edinburgh SEELLD Personal Fellowship. NMK wishes to thank S.L. Harley for valuable discussions and revisions of the content of this manuscript. Some imaging of zircons was completed at the University of Edinburgh with the assistance of N. Cayzer.

8. References

Asami, M., Suzuki, K., Grew, E. S. 2002. Chemical Th-U-total Pb dating by electron microprobe analysis of monazite, xenotime and zircon from the Archaean Napie Complex, East Antarctica: evidence for ultra-high-temperature metamorphism at 2400 Ma. *Precambrian Research* **114**, 249–75.

Black, L. P. & James, P. R. 1982. Geological History of the Archaean Napier Complex in Enderby Land. *In* Oliver, R. L., James, P. R. & Jago, J. B. (eds) *Antarctic Earth Science*, 11–15. Australian Academy of Science and Cambridge: Cambridge University Press.

Black, L. P., James, P. R. & Harley, S. L. 1983. Geochronology, structure, and metamorphism of early Archaean rocks at Fyfe Hills, Enderby Land, Antarctica. *Precambrian Research* **21**, 197–222.

Black, L. P., Williams, I. S. & Compston, W. 1986. Four zircon ages from one rock: the history of a 3930 Ma-old granulite from Mount Sones, Enderby Land, Antarctica. *Contributions to Mineralogy and Petrology* **94**, 427–37

Black, L. P., Harley, S. L., Sun, S. S. & McCulloch, M. T. 1987. The Rayner Complex of east Antarctica: complex isotopic systematics within a Proterozoic mobile belt. *Journal of Metamorphic Geology* **5**, 1–26.

Boger, S. D., Carson, C. J., Wilson, C. J. L. & Fanning, C. M. 2000. Neoproterozoic deformation in the Radok Lake region of the northern Prince Charles Mountains, east Antarctica; evidence for a single protracted orogenic event. *Precambrian Research* **104**, 1–24.

Carson, C. J., Boger, S. D., Fanning, C. M., Wilson, C. J. L. & Thost, D. E. 2000a. Shrimp U-Pb geochronology from Mt Kirkby, northern Prince Charles Mountains, east Antarctica. *Antarctic Science* **12**, 429–42.

Carson, C. J., Ague, J. J., Grove, M., Coath, C. D. & Harrison, T. M. 2002b. U-Pb isotopic behaviour of zircon during upper-amphibolite facies fluid infiltration in the Napier Complex, east Antarctica. *Earth and Planetary Sciences* **199**, 287–310.

Carson, C. J., Ague, J. J. & Coath, C. D. 2002c. U-Pb geochronology from Tonagh Island, East Antarctica: implications for the timing of ultra-high temperature metamorphism of the Napier Complex. *Precambrian Research* **116**, 237–63.

Cherniak, D. J., Lanford, W. A. & Ryerson, F. J. 1991. Lead diffusion in apatite and zircon using ion implantation and Rutherford Backscattering techniques. *Geochimica et Cosmochimica Acta* **55**, 1663–73.

Claoué-Long, J. C., Compston, W., Roberts, J. & Fanning, C. M. 1995. Two Carboniferous ages: a comparison of Shrimp zircon dating with conventional zircon ages and $^{40}Ar/^{39}Ar$ analysis. *In* Berggren, W. A., Kent, D. V., Aubrey, M.-P. & Hardenbol, J. (eds) *Geochronology Time Scales and Global Stratigraphic Correlation, SEPM Special Publication* **54**, 3–21, Tulsa, Oklahoma: Society for Sedimentary Geology.

Clarke, G. L. 1987. *A comparative study of the structural and metamorphic evolution of the Olary (South Australia) and Stillwell Hills (Antarctica) Precambrian terrains*. Unpublished PhD thesis, University of Melbourne, Australia.

Crowe W. A., Osanai Y., Toyoshima T., Owada M., Tsunogae T. & Hokada T. 2002. SHRIMP geochronology of a mylonite zone on Tonagh Island: characterisation of the last high-grade tectono-thermal event in the Napier Complex, East Antarctica. *Polar Geoscience* **15**, 17–36.

Dunkley, D. J. 1998. *The Rayner Complex in MacRobertson Land, east Antarctica*. Unpublished PhD thesis, University of Sydney, Sydney, Australia.

Dunkley, D. J., Clarke, G. L. & White R. W. 2003. The ~1020–900 Ma Rayner Structural Episode in MacRobertson Land, east Antarctica: a case of oblique continental collision? Proceedings of the 8th International Symposium on Antarctic Earth Sciences, Wellington, New Zealand, 1999. *The Royal Society of New Zealand Bulletin* **35**, 31–42

Fitzsimons, I. C. W. 2000. A review of tectonic events in the East Antarctic Shield and their implications for Gondwana and earlier supercontinents. *Journal of African Earth Sciences* **31**, 2–23.

Fraser, G., Ellis, D. & Eggins, S. 1997. Zirconium abundance in granulite-facies minerals, with implications for zircon geochronology in high-grade rocks. *Geology* **25**, 607–10.

Geisler, T., Pidgeon, R. T., van Bronswijk, W. & Kurtz, R. 2002. Transport of uranium, thorium and lead in metamict zircon under low-temperature hydrothermal conditions. *Chemical Geology* **191**, 141–54.

Grew, E. S. 1978. Precambrian basement at Molodezhnaya Station, east Antarctica. *Geological Society of America Bulletin* **89**, 801–13.

Grew, E. S. & Manton, W. 1979. Archaean rocks in Antarctica: 2·5 billion year uranium-lead ages of pegmatites in Enderby Land. *Science* **206**, 443–5.

Grew, E. S. & Manton, W. I. 1986. A new correlation of sapphirine granulites in the Indo-Antarctic metamorphic terrain: late Proterozoic dates from the Eastern Ghats Province of India. *Precambrian Research* **33**, 123–37.

Grew, E. S., Manton, W. & Sandiford, M. 1982. Geochronologic studies in East Antarctica: age of pegmatites in Casey Bay, Enderby Land. *Antarctic Journal of the United States* **17**, 1–2.

Hanchar, J. M. & Miller, C. F. 1993. Zircon zonation patterns as revealed by cathodoluminescence and backscattered electron images: Implications for interpretation of complex crustal histories. *Chemical Geology* **110**, 1–13.

Hanchar, J. M. & Rudnick, R. L. 1995. Revealing hidden structures: the application of cathodoluminescence and back-scattered electron imaging to dating zircons from lower crustal xenoliths. *Lithos* **36**, 289–303.

Harley, S. L. 2001. Zircon chemistry and the definition of high-grade events in East Antarctica. *Journal of Conference Abstracts* **6**(1), 375.

Harley, S. L. & Hensen, B. J. 1990. Archaean and Proterozoic high-grade terranes of east Antarctica (40–80°): a case study of diversity in granulite facies metamorphism. *In* Ashworth, J. R. & Brown, M. (eds) *High-temperature Metamorphism and Crustal Anatexis. Mineralogical Society Special Publication* **2**, 320–70. London: Unwin Hyman.

Harley, S. L. & Black, L. P. 1997. A revised Archaean chronology for the Napier Complex, Enderby Land, from SHRIMP ion-microprobe studies. *Antarctic Science* **9**, 74–91.

Harley, S. L., Snape, I. & Black, L. P. 1998. The evolution of a layered metaigneous complex in the Rauer Group, East Antarctica: evidence for a distinct Archaean terrane. *Precambrian Research* **89**, 175–205.

Harrison, T. M., Aleinikoff, J. N. & Compston, W. 1987. Observations and controls on the occurrence of inherited zircon in Concord-type granitoids, New Hampshire. *Geochimica et Cosmochimica Acta* **52**, 2549–58.

Hartmann, L. A., Takehara, L., Leite, J. A. D., McNaughton, N. J. & Vasconcellos, M. A. Z. 1997. Fracture sealing in zircon as evaluated by electron microprobe analyses and back-scattered electron imaging. *Chemical Geology* **141**, 67–72.

Hermann, J., Rubatto, D., Korsakov, A. & Shatsky, V. S. 2001. Multiple zircon growth during fast exhumation of diamondiferous, deeply subducted continental crust (Kokchetav Massif, Kazakhstan). *Contributions to Mineralogy and Petrology* **141**, 66–82.

Hokada T., Misawa K., Kazuyuki S. & Suzuki S. 2003. Mid to late Archaean (3·3–2·5 Ga) tonalitic crustal formation and high-grade metamorphism at Mt Riiser-Larsen, Napier Complex, east Antarctica. *Precambrian Research* **127**, 215–28.

Hoskin, P. W. O. & Black, L. P. 2000. Metamorphic zircon formation by solid state recrystallisation of protolith igneous zircon. *Journal of Metamorphic Geology* **18**, 423–39.

Kamenev, E. N. 1972. Geological structure of Enderby Land. *In* Adie, R. J. (ed.) *Antarctic Geology and Geophysics*, 579–83. Oslo, Norway: Universitetsforlaget.

Kelly, N. M. & Harley, S. L. 2005. An integrated microtextural and chemical approach to zircon geochronology: refining the Archaean history of the Napier Complex, east Antarctica. *Contributions to Mineralogy and Petrology*, in press.

Kelly, N. M., Clarke, G. L., Carson, C. J. & White, R. W. 2000. Thrusting in the lower crust: evidence from the Oygarden Islands, Kemp Land, East Antarctica. *Geological Magazine* **137**, 219–34.

Kelly, N. M., Clarke, G. L. & Fanning, C. M. 2002. A two-stage evolution of the Neoproterozoic Rayner Structural Episode: new U-Pb SHRIMP constraints from the Oygarden Group, Kemp Land, East Antarctica. *Precambrian Research* **116**, 307–30.

Kinny, P. D. 1987. *An ion microprobe study of U-Pb and hafnium isotopes in natural zircon*. PhD thesis, Australian National University.

Kinny, P. D., Black, L. P. & Sheraton, J. W. 1997. Zircon U-Pb ages and geochemistry of igneous and metamorphic rocks from the northern Prince Charles Mountains, Antarctica. *AGSO Journal of Australian Geology and Geophysics* **16**, 637–54.

Koschek, G. 1993. Origin and significance of SEM cathodoluminescence from zircon. *Journal of Microscopy* **171**, 223–32.

Ludwig, K. R. 1999. User manual for Isoplot/Ex, version 2.10, a geochronological toolkit for Microsoft Excel. *Berkley Geochronological Centre Special Publication 1a.*

Manton, W. I., Grew, E. S., Hofmann, J. & Sheraton, J. W. 1992. Granitic rocks of the Jetty Peninsula, Amery Ice Shelf area, east Antarctica. *In* Yoshida, Y., Kaminuma, K. & Shiraishi, K. (eds) *Recent Progress in Antarctic Earth Science*, 179–89. Tokyo: Terra Scientific Publishing Company.

Mattinson, J. M., Graubard, C. M., Parkinson, D. L. & McClelland, W. C. 1996. U-Pb reverse discordance in zircons: the role of fine-scale oscillatory zoning and sub-micron transport of Pb. *In* Basu, A. & Hart, S. (eds) *Earth Processes: Reading the Isotopic Code. Geophysical Monograph* **95**, 355–76.

McLaren, A. C., Fitzgerald, J. D. & Williams, I. S. 1994. The microstructure of zircon and its influence on the age determination from Pb/U isotopic ratios measured by ion microprobe. *Geochimica et Cosmochimica Acta* **58**, 993–1005.

Meldrum, A., Boatner, L. A., Weber, W. J. & Ewing, R. C. 1998. Radiation damage in zircon and monazite. *Geochimica et Cosmochimica Acta* **62**, 2509–20.

Mezger, K. & Krogstad, E. J. 1997. Interpretation of discordant U-Pb zircon ages: An evaluation. *Journal of Metamorphic Geology* **15**, 127–40.

Mezger, K. & Cosca, M. A. 1999. The thermal history of the Eastern Ghats Belt (India) as revealed by U-Pb and $^{40}Ar/^{39}Ar$ dating of metamorphic and magmatic minerals: implications for the SWEAT correlation. *Precambrian Research* **94**, 251–71.

Mikhalsky, E. V., Sheraton, J. W., Laiba, A. A. & Beliatsky, B. V. 1996. Geochemistry and origin of Mesoproterozoic metavolcanic rocks from Fisher Massif, Prince Charles Mountains, east Antarctica. *Antarctic Science* **8**, 85–104.

Muir, R. J., Ireland, T. R., Weaver, S. D. & Bradshaw, J. D. 1996. Ion microprobe dating of Paleozoic granitoids; Devonian magmatism and correlations with Australia and Antarctica. *Chemical Geology* **127**, 191–210.

Paces, J. B. & Miller, J. D. 1993. Precise U-Pb ages of Duluth Complex and related mafic intrusions, northeastern Minnesota: Geochronological insights into physical, petrogenetic, palaeomagnetic, and tectonomagmatic processes associated with the 1·1 Ga midcontinent rift system. *Journal of Geophysical Research* **98**, 13,997–14,013.

Pidgeon, R. T. 1992. Recrystallisation of oscillatory zoned zircon: some geochronological and petrological implications. *Contributions to Mineralogy and Petrology* **110**, 463–72.

Pidgeon, R. T., Nemchin, A. A. & Hitchen, J. G. 1998. Internal structures of zircons from Archaean granites from the Darling Range batholith: implications for zircon stability and the interpretation of zircon U-Pb ages. *Contributions to Mineralogy and Petrology* **132**, 288–99.

Rickers, K., Mezger, K. & Raith, M. M. 2001. Evolution of the continental crust in the Proterozoic Eastern Ghats Belt, India and new constraints for Rodinia reconstruction: implications from Sm-Nd, Rb-Sr and Pb-Pb isotopes. *Precambrian Research* **112**, 183–210.

Roberts, M. & Finger, F. 1997. Do U-Pb zircon ages from granulites reflect peak metamorphic conditions? *Geology* **18**, 1207–10.

Rubatto, D. & Gebauer, D. 2000. Use of cathodoluminescence for U-Pb zircon dating by ion microprobe: some examples from the Western Alps. *In* Pagel, M., Barbin, V., Blanc, P. & Ohnenstetter, D. (eds) *Cathodoluminescence in Geoscience*, 374–400. Berlin: Springer-Verlag.

Rubatto, D., Gebauer, D. & Fanning, M. 1998. Jurassic formation and Eocene subduction of the Zermatt-Saas-Fee ophiolites: implications for the geodynamic evolution of the Central and Western Alps. *Contributions of Mineralogy and Petrology* **132**, 269–87.

Rubatto, D., Gebauer, D. & Compagnoni, R. 1999. Dating of eclogite-facies zircons: the age of Alpine metamorphism in the Sesia-Lanzo Zone (Western Alps). *Earth and Planetary Science Letters* **167**, 141–58.

Sandiford, M. & Wilson, C. J. L. 1984. The structural evolution of the Fyfe Hills-Khmara Bay region, Enderby Land, east Antarctica. *Australian Journal of Earth Sciences* **31**, 403–26.

Schaltegger, U., Fanning, C. M., Günther, D., Maurin, J. C., Schulmann, K. & Gebauer, D. 1999. Growth, annealing and recrystallisation of zircon and preservation of monazite in high-grade metamorphism: conventional and in-situ U-Pb isotope, cathodoluminescence and microchemical. *Contributions to Mineralogy and Petrology* **134**, 186–201.

Sheraton, J. W. & Black, L. P. 1983. Geochemistry of Precambrian gneisses: relevance for the evolution of the East Antarctic Shield. *Lithos* **16**, 273–96.

Sheraton, J. W., Tingey, R. J., Black, L. P., Offe, L. A. & Ellis, D. J. 1987. Geology of an unusual Precambrian high-grade metamorphic terrane – Enderby Land and western Kemp Land, Antarctica. *Australian Bureau of Mineral Resources Bulletin* **223**.

Sheraton, J. W., Tindle, A. G. & Tingey, R. J. 1996. Geochemistry, origin, and tectonic setting of granitic rocks of the Prince Charles Mountains, Antarctica. *AGSO Journal of Australian Geology and Geophysics* **16**, 345–70.

Shiraishi, K., Ellis, D. J., Fanning, C. M., Hiroi, Y., Kagami, H. & Motoyoshi, Y. 1997. Re-examination of the metamorphic and protolith ages of the Rayner Complex, Antarctica: evidence for the Cambrian (Pan-African) regional metamorphic event. *In* Ricci, C. A. (ed.) *The Antarctic Region: Geological Evolution and Processes*, 79–88. Siena: Terra Antarctica Publications.

Tingey, R. J. 1991. The regional geology of Archaean and Proterozoic rocks in Antarctica. *In* Tingey, R. J. (ed.) *The Geology of Antarctica*, 1–73. Oxford: Oxford University Press.

Tomaschek, F., Kennedy, A. K., Villa, I. M., Lagos, M. & Ballhaus, C. 2003. Zircons from Syros, cyclades, Greece – recrystallisation and mobilisation of zircon during high-pressure metamorphism. *Journal of Petrology* **44**, 1977–2002.

Trail, D. S. 1970. ANARE 1961 Geological traverses on the MacRobertson Land and Kemp Land Coast. *Bureau of Mineral Resources, Geology and Geophysics, Report* **135**.

Vavra, G. 1990. On the kinematics of zircon growth and its petrogenetic significance: a cathodoluminescence study. *Contributions to Mineralogy and Petrology* **106**, 90–9.

Vavra, G., Gebauer, D., Schmid, R. & Compston, W. 1996. Multiple zircon growth and recrystallisation during polyphase Late Carboniferous to Triassic metamorphism in granulites of Ivrea Zone (Southern Alps): an ion microprobe (SHRIMP) study. *Contributions to Mineralogy and Petrology* **122**, 337–58.

Vavra, G., Schmid, R. & Gebauer, D. 1999. Internal morphology, habit and U-Th-Pb microanalysis of amphibolite-to-granulite facies zircons: geochronology of the Ivrea Zone (Southern Alps). *Contributions to Mineralogy and Petrology* **143**, 380–404.

Watson, E. B. & Liang, Y. 1995. A simple model for sector zoning in slowly grown crystals: implications for growth rate and lattice diffusion, with emphasis on accessory minerals in crustal rocks. *American Mineralogist* **80**, 1179–87.

Wiedenbeck, M. 1995. An example of reverse discordance during ion microprobe zircon dating: An artifact of enhanced ion yields from a radiogenic labile Pb. *Chemical Geology* **125**, 197–218.

Williams, I. S. 1992. Some observations on the use of zircon U-Pb geochronology in the study of granitic rocks. *Transactions of the Royal Society of Edinburgh: Earth Sciences* **83**, 447–58.

Williams, I. S. 1998. U-Th-Pb geochronology by ion microprobe. *Reviews in Economic Geology* **7**, 1–35.

Williams, I. S., Compston, W., Black, L. P., Ireland, T. R. & Foster, J. J. 1984. Unsupported radiogenic Pb in zircon: a cause of anomalously high Pb-Pb, U-Pb, and Th-Pb ages. *Contributions to Mineralogy and Petrology* **88**, 322–7.

Yoshida, M., Santosh, M. & Arima, M. 1996. Precambrian India within East Gondwana: Introduction. *Journal of Southeast Asian Earth Sciences* **14**, 117–18.

Young, D. N. & Black, L. P. 1991. U-Pb zircon dating of Proterozoic igneous charnockites from the Mawson coast, east Antarctica. *Antarctic Science* **3**, 205–16.

Young, D. N., Zhao, J. -x., Ellis, D. J. & McColloch, M. T. 1997. Geochemical and Sr-Nd isotopic mapping of source provinces for the Mawson charnockites, east Antarctica: implications for Proterozoic tectonics and Gondwana reconstruction. *Precambrian Research* **86**, 1–19.

Zeck, H. P. & Whitehouse, M. J. 1999. Hercynian, Pan-African, Proterozoic and Archaean ion-microprobe zircon ages for a Btic-Rif core complex, Alpine belt, W Mediterranean – consequences for its P-T-t path. *Contributions to Mineralogy and Petrology* **134**, 134–49.

Zhao, J.-x., Ellis, D. J., Kilpatrick, A. & McColloch, M. T. 1997. Geochemical and Sr-Nd isotopic study of charnockites and related rocks in the northern Prince Charles Mountains, east Antarctica: implications for charnockite petrogenesis and Proterozoic crustal evolution. *Precambrian Research* **81**, 37–66.

N. M. KELLY* and G. L. CLARKE, School of Geosciences, F05, University of Sydney, NSW 2006, Australia.

C. M. FANNING, Research School of Earth Sciences, The Australian National University, ACT 0200, Australia.
*Current address: School of Geosciences, University of Edinburgh, West Mains Road, Edinburgh EH9 3JW, Scotland, UK.

MS received 23 December 2003. Accepted for publication 18 January 2005.